

A hyperbolicity-preserving discontinuous stochastic Galerkin scheme for uncertain hyperbolic systems of equations

Jakob Dürrwächter^a, Thomas Kuhn^b, Fabian Meyer^c, Louisa Schlachter^d, Florian Schneider^e

^a*Institut für Aerodynamik und Gasdynamik, Universität Stuttgart, Pfaffenwaldring 21, 70569 Stuttgart, Germany, jakob.duerrwaechter@iag.uni-stuttgart.de*

^b*Institut für Aerodynamik und Gasdynamik, Universität Stuttgart, Pfaffenwaldring 21, 70569 Stuttgart, Germany, thomas.kuhn@iag.uni-stuttgart.de*

^c*Institut für Angewandte Analysis und numerische Simulation, Universität Stuttgart, Pfaffenwaldring 57, 70569 Stuttgart, Germany, fabian.meyer@mathematik.uni-stuttgart.de*

^d*Fachbereich Mathematik, TU Kaiserslautern, Erwin-Schrödinger-Str., 67663 Kaiserslautern, Germany, schlacht@mathematik.uni-kl.de*

^e*Fachbereich Mathematik, TU Kaiserslautern, Erwin-Schrödinger-Str., 67663 Kaiserslautern, Germany, schneider@mathematik.uni-kl.de*

Abstract

Intrusive Uncertainty Quantification methods such as stochastic Galerkin are gaining popularity, whereas the classical stochastic Galerkin approach is not ensured to preserve hyperbolicity of the underlying hyperbolic system. We apply a modification of this method that uses a slope limiter to retain admissible solutions of the system, while providing high-order approximations in the physical and stochastic space. This is done using a spatial discontinuous Galerkin scheme and a Multi-Element stochastic Galerkin ansatz in the random space. We analyze the convergence of the resulting scheme and apply it to the compressible Euler equations with various uncertain initial states in one and two spatial domains with up to three uncertainties. The performance in multiple stochastic dimensions is compared to the non-intrusive Stochastic Collocation method. The numerical results underline the strength of our method, especially if discontinuities are present in the uncertainty of the solution.

Keywords: Uncertainty Quantification, Polynomial chaos, stochastic Galerkin, discontinuous Galerkin, Hyperbolicity, Multi-Element

2010 MSC: 35L60, 35Q31, 35Q62, 37L65, 65M08, 65M60

1. Introduction

Non-deterministic effects may influence the validity of accurate approximations of deterministic systems because uncertain inputs in parameters, initial or boundary conditions yield a propagation of the uncertainty into the solution. Therefore, it is important to account for these uncertainties and hence Uncertainty Quantification (UQ) is becoming more and more important in numerical simulations. The two main sources for these non-deterministic effects (or uncertainties) are the limitations in measuring physical parameters exactly and the absence of knowledge of the underlying physical processes.

In general there exist two major approaches to quantify the influence of uncertain parameters, see for example [1, 15, 16, 23, 30] for a general overview of different UQ methods. Statistical approaches such as (multilevel) Monte Carlo (MC) type methods [19–22] sample the random space to obtain statistical information, like

mean, variance or higher-order moments of the corresponding random field. While they are very robust even for non-smooth problems like solutions of hyperbolic systems, they suffer from a slow rate of convergence dictated by the law of large numbers. In contrast, non-statistical approaches, like the intrusive and non-intrusive Polynomial Chaos (PC) expansion, or the Stochastic Collocation method, approximate the random field by a series of polynomials and derive deterministic models for the stochastic modes. The theoretical foundation for the PC expansion has been laid in [37] and can be described as a polynomial approximation of Gaussian random variables to represent random processes. Later, the approach has been generalized to a larger class of distributions [41], which is now known as generalized Polynomial Chaos (gPC). The intrusive PC expansion, also known as stochastic Galerkin (SG) approach, considers a weak formulation of the partial differential equation with respect to the stochastic variable and uses corresponding orthonormal polynomials as ansatz and test functions.

For many random elliptic and parabolic equations, the underlying random field is sufficiently smooth with respect to the stochastic variable and hence the use of the SG method is superior compared to MC methods. This is mainly due to the fact that the gPC approximation exhibits spectral convergence [3, 11, 42]. However, the naive usage of the stochastic Galerkin (SG) approach for nonlinear hyperbolic problems typically fails [1, 25] since the polynomial expansion of discontinuous data leads to huge oscillations (also known as Gibbs phenomenon). In the case of nonlinear systems of conservation laws, the resulting SG system might even lose its hyperbolicity.

To reduce the Gibbs oscillations, the authors of [34] developed the so-called Multi-Element method which subdivides the random space into smaller, disjoint elements. This corresponds to an h -refinement in the random space. Further developments of the Multi-Element approach encompass h - and hp -adaptive refinements in the stochastic space ([33, 34, 36]) or a multi-resolution discretization using wavelets instead of gPC, cf. [6, 24]. Another approach which ensures hyperbolicity of the resulting nonlinear SG system is the intrusive polynomial moment method. It bounds the oscillations of the Gibbs phenomenon by expanding the stochastic solution not in the conserved variables but in so-called entropic variables [25], which is well known in the radiative transfer community as minimum entropy models [5, 17, 18]. The resulting SG system is hyperbolic and has good approximation properties but requires to solve (typically) expensive nonlinear systems in every space-time cell. Furthermore, it is necessary that the system possesses a strictly convex entropy function, which has to be known beforehand to define the entropic variables.

In this article, we extend the hyperbolicity-preserving limiter developed in [27] to (spatial) discontinuous Galerkin (DG) schemes ensuring the hyperbolicity of the resulting DG-SG system. Moreover, we combine the limiter with the Multi-Element approach to further decrease Gibbs oscillations and ensure a high-order approximation in both physical and stochastic space. We compare the performance of our numerical scheme to that of the non-intrusive Stochastic Collocation method for a smooth solution. In less than three stochastic dimensions our method proves to be more efficient than the Stochastic Collocation method. Furthermore, we apply our method to different one- and two-dimensional Riemann problems for the compressible Euler equations, which shows that our method is able to handle complex flow problems.

The rest of the paper is organized as follows. In Section 2 we describe our hyperbolic model problem and the classical stochastic Galerkin approach. Moreover, we explain the Multi-Element approach and define the domain of hyperbolicity. Our modification of the SG method combined with DG and the hyperbolicity-preserving limiter is stated in Section 3, where we also prove its hyperbolicity-preservation and embed the two-dimensional compressible Euler equations into our framework. Section 4 is devoted to a numerical convergence analysis and applications to the compressible Euler equations with different uncertain initial states in multiple stochastic dimensions, which we extensively investigate numerically.

2. Uncertainty Quantification

Throughout this paper, we restrict ourselves to the study of two-dimensional random systems of hyperbolic conservation laws of the form

$$\partial_t \mathbf{u} + \partial_x \mathbf{f}_1(\mathbf{u}) + \partial_y \mathbf{f}_2(\mathbf{u}) = 0, \quad (2.1)$$

with flux components $\mathbf{f}_i(\mathbf{u}) : \mathbb{R}^d \rightarrow \mathbb{R}^d$, $i = 1, 2$ in two spatial dimension $(x, y)^\top \in \mathcal{X} \subset \mathbb{R}^2$, and where the solution

$$\mathbf{u} = \mathbf{u}(t, x, y, \boldsymbol{\xi}) : \mathbb{R}_+ \times \mathbb{R}^2 \times \Omega \rightarrow \mathbb{R}^d$$

is depending on an N -dimensional real-valued random vector $\boldsymbol{\xi} = (\xi^1, \dots, \xi^N)$ defined on a probability space $(\Omega, \mathcal{F}, \mathbb{P})$. We assume that the entries of $\boldsymbol{\xi}$ are independent, identically distributed random variables. We denote the image of the random vector by $\Gamma := \boldsymbol{\xi}(\Omega) \subset \mathbb{R}^N$ and its probability density function by $f_\Xi(\boldsymbol{\xi}) : \Gamma \rightarrow \mathbb{R}_+$. Due to the independence of the entries of $\boldsymbol{\xi}$ we may write $f_\Xi(\boldsymbol{\xi}) = \prod_{n=1}^N f_{\Xi_n}(\xi^n)$, where f_{Ξ_n} is the probability density function of the random variable ξ^n , for $n = 1, \dots, N$. We further assume that the uncertainty is introduced via the initial conditions, namely

$$\mathbf{u}(t = 0, x, y, \boldsymbol{\xi}) = \mathbf{u}^0(x, y, \boldsymbol{\xi}).$$

We solve the system (2.1) using a Runge–Kutta time-stepping method combined with a discontinuous Galerkin method in space (see Section 3). The stochastic discretization uses the generalized Polynomial Chaos (gPC) theory [37, 41], which will be explained by the following stochastic Galerkin approach.

2.1. Stochastic Galerkin

The stochastic Galerkin (SG) method discretizes Γ by a suitable orthonormal basis. For a multi-dimensional $\Gamma \subset \mathbb{R}^N$, we first introduce the family of multivariate orthonormal polynomials. To this end we consider the one-dimensional orthonormal polynomials $(\phi_\kappa(\xi^n))_{\kappa=0, \dots, \infty}$, $n = 1, \dots, N$, w.r.t. to the inner product induced by the probability density function f_{Ξ_n} , i.e.,

$$\langle \mathbf{h}(\xi^n), \mathbf{g}(\xi^n) \rangle_{\Gamma_n} := \int_{\omega \in \Omega} \mathbf{h}(\xi^n(\omega)) \mathbf{g}(\xi^n(\omega)) d\mathbb{P}(\omega) = \int_{\xi^n \in \Gamma_n} \mathbf{h}(\xi^n) \mathbf{g}(\xi^n) f_{\Xi_n}(\xi^n) d\xi^n, \quad (2.2)$$

where $\Gamma_n := \xi^n(\Omega)$. Thus, $(\phi_\kappa(\xi^n))_{\kappa=0, \dots, \infty}$ form a basis of the (weighted) space $L_2(\Gamma_n)$. For any multi-index $\kappa = (\kappa_1, \dots, \kappa_N)^\top \in \mathbb{N}_0^N$, we define the multivariate orthonormal polynomials $\phi_\kappa(\boldsymbol{\xi}) := \phi_{\kappa_1}(\xi^1) \dots \phi_{\kappa_N}(\xi^N)$. According to [41], we can write \mathbf{u} as the Fourier series

$$\mathbf{u}(t, x, y, \boldsymbol{\xi}) = \sum_{\kappa \in \mathbb{N}_0^N} \mathbf{u}_\kappa(t, x, y) \phi_\kappa(\boldsymbol{\xi}), \quad (2.3)$$

with deterministic coefficients \mathbf{u}_κ . The solution \mathbf{u} of (2.1) is now approximated by truncating the infinite sum (2.3) at finite order K_Γ . In the following we consider the complete polynomial space described by the following index set $\kappa \in \mathcal{K} := \{\kappa = (\kappa_1, \dots, \kappa_N)^\top \in \mathbb{N}_0^N \mid \sum_{n=1}^N \kappa_n \leq K_\Gamma\}$, cf. [40]. Hence, the SG approximation reads as follows

$$\mathbf{u} \approx \sum_{\kappa \in \mathcal{K}} \mathbf{u}_\kappa(t, x, y) \phi_\kappa(\boldsymbol{\xi}), \quad (2.4)$$

which, by the Cameron–Martin theorem [7], is converging to (2.3) in $L_2(\Gamma)$, as $K_\Gamma \rightarrow \infty$. The polynomial moments \mathbf{u}_κ of \mathbf{u} are determined by the Galerkin projection, given by

$$\mathbf{u}_\kappa(t, x, y) = \int_\Gamma \mathbf{u}(t, x, y, \boldsymbol{\xi}) \phi_\kappa(\boldsymbol{\xi}) f_\Xi d\boldsymbol{\xi}. \quad (2.5)$$

We insert the ansatz (2.4) into the system of conservation laws (2.1) and project the result onto the complete polynomial space. We then obtain

$$\partial_t \int_{\Gamma} \left(\sum_{\kappa \in \mathcal{K}} \mathbf{u}_{\kappa} \phi_{\kappa} \right) \phi_j f_{\Xi} d\boldsymbol{\xi} + \partial_x \int_{\Gamma} \mathbf{f}_1 \left(\sum_{\kappa \in \mathcal{K}} \mathbf{u}_{\kappa} \phi_{\kappa} \right) \phi_j f_{\Xi} d\boldsymbol{\xi} + \partial_y \int_{\Gamma} \mathbf{f}_2 \left(\sum_{\kappa \in \mathcal{K}} \mathbf{u}_{\kappa} \phi_{\kappa} \right) \phi_j f_{\Xi} d\boldsymbol{\xi} = 0, \quad j \in \mathcal{K}.$$

The orthonormality of the basis functions yields the following stochastic Galerkin system

$$\underbrace{\partial_t \begin{pmatrix} \mathbf{u}_0 \\ \vdots \\ \mathbf{u}_{N_{K_{\Gamma}}} \end{pmatrix}}_{=: \mathbf{U}} + \underbrace{\partial_x \begin{pmatrix} \int_{\Gamma} \mathbf{f}_1 (\sum_{\kappa \in \mathcal{K}} \mathbf{u}_{\kappa} \phi_{\kappa}) \phi_0 f_{\Xi} d\boldsymbol{\xi} \\ \vdots \\ \int_{\Gamma} \mathbf{f}_1 (\sum_{\kappa \in \mathcal{K}} \mathbf{u}_{\kappa} \phi_{\kappa}) \phi_{N_{K_{\Gamma}}} f_{\Xi} d\boldsymbol{\xi} \end{pmatrix}}_{=: \mathbf{F}_1(\mathbf{U})} + \underbrace{\partial_y \begin{pmatrix} \int_{\Gamma} \mathbf{f}_2 (\sum_{\kappa \in \mathcal{K}} \mathbf{u}_{\kappa} \phi_{\kappa}) \phi_0 f_{\Xi} d\boldsymbol{\xi} \\ \vdots \\ \int_{\Gamma} \mathbf{f}_2 (\sum_{\kappa \in \mathcal{K}} \mathbf{u}_{\kappa} \phi_{\kappa}) \phi_{N_{K_{\Gamma}}} f_{\Xi} d\boldsymbol{\xi} \end{pmatrix}}_{=: \mathbf{F}_2(\mathbf{U})} = 0, \quad (2.6)$$

with \mathbf{U} , $\mathbf{F}_{\alpha}(\mathbf{U}) \in \mathbb{R}^{dN_{K_{\Gamma}}}$, for $\alpha = 1, 2$, where $N_{K_{\Gamma}} := \binom{N+K_{\Gamma}}{N}$ is the number of basis polynomials. The Jacobian matrix of this model reads

$$\frac{\partial \mathbf{F}^{\alpha}}{\partial \mathbf{U}} = \begin{pmatrix} \hat{\mathbf{F}}_{00}^{\alpha} & \cdots & \hat{\mathbf{F}}_{0N_{K_{\Gamma}}}^{\alpha} \\ \vdots & & \vdots \\ \hat{\mathbf{F}}_{N_{K_{\Gamma}}0}^{\alpha} & \cdots & \hat{\mathbf{F}}_{N_{K_{\Gamma}}N_{K_{\Gamma}}}^{\alpha} \end{pmatrix} \in \mathbb{R}^{dN_{K_{\Gamma}} \times dN_{K_{\Gamma}}}, \quad (2.7)$$

where

$$\hat{\mathbf{F}}_{ji}^{\alpha} = \int_{\Gamma} \frac{\partial \mathbf{f}_{\alpha}}{\partial \mathbf{u}} \left(\sum_{\kappa \in \mathcal{K}} \mathbf{u}_{\kappa} \phi_{\kappa} \right) \phi_j \phi_i f_{\Xi} d\boldsymbol{\xi} \in \mathbb{R}^{d \times d}, \quad i, j = 0, \dots, N_{K_{\Gamma}},$$

for $\alpha = 1, 2$. The deterministic stochastic Galerkin system (2.6) can then be solved by any suitable numerical method. We will focus on the RKDG method, which will be described in detail in Section 3.1.

2.2. Multi-Element Stochastic Galerkin

A major drawback of the plain SG approach for hyperbolic conservation laws is that for a discontinuous solution, the gPC approach may converge slowly or even fail to converge, due to Gibbs oscillations, cf. [25, 34]. To overcome this issue we employ the Multi-Element (ME) approach as presented in [35], where we subdivide Γ into disjoint elements and consider a local gPC approximation of (2.1) on every random element.

For ease of presentation we assume that $\Gamma = [0, 1]^N$, and let $0 = d_1 < d_2 < \dots < d_{N_{\Gamma}+1} = 1$ be a decomposition of $[0, 1]$. We define $D_n := [d_n, d_{n+1})$, for $n = 1, \dots, N_{\Gamma} - 1$, and $D_{N_{\Gamma}} := [d_{N_{\Gamma}}, d_{N_{\Gamma}+1}]$. Introducing the tensor-product index set $\mathcal{L} := \{l = (l_1, \dots, l_N)^{\top} \in \mathbb{N}_0^N : l_n \leq N_{\Gamma}, n = 1, \dots, N\}$ allows us to define the Multi-Element $D_l := \bigtimes_{n=1}^N D_{l_n}$ with $\Delta \boldsymbol{\xi} := \prod_{n=1}^N (d_{l_n+1} - d_{l_n})$ and $l \in \mathcal{L}$. Moreover, we introduce an indicator variable $\chi_l : \Omega \rightarrow \{0, 1\}$ on every random element

$$\chi_l(\boldsymbol{\xi}(\omega)) := \begin{cases} 1, & \text{if } \boldsymbol{\xi}(\omega) \in D_l, \\ 0, & \text{else,} \end{cases} \quad (2.8)$$

for $l \in \mathcal{L}$. Using the indicator variable allows us to derive a disjoint partition of the sample space Ω via

$$\Omega = \bigcup_{l \in \mathcal{L}} \chi_l^{-1}(1).$$

Hence, we can define a new local random vector $\boldsymbol{\xi}_l = (\xi_l^1, \dots, \xi_l^N) : \chi_l^{-1}(1) \rightarrow D_l$ on the local probability space $(\chi_l^{-1}(1), \mathcal{F} \cap \chi_l^{-1}(1), \mathbb{P}(\cdot | \chi_l(\boldsymbol{\xi}) = 1))$. Using Bayes' rule we compute the following local probability density functions

$$f_{D_l} := f_{D_l}(\boldsymbol{\xi}_l | \chi_l(\boldsymbol{\xi}) = 1) = \frac{f_{\Xi}(\boldsymbol{\xi}_l)}{\mathbb{P}(\chi_l(\boldsymbol{\xi}) = 1)}. \quad (2.9)$$

Remark 2.1. For a uniform distribution we have $f_{D_l} = \prod_{n=1}^N \frac{1}{d_{l_n+1} - d_{l_n}}$.

If we let $\{\phi_{\kappa,l}(\xi_l)\}_{\kappa \in \mathbb{N}_0^N}$ be the orthonormal polynomials with respect to the conditional probability density function (2.9), we may consider the local gPC approximation in element D_l ,

$$\mathbf{u}_l(t, x, y, \xi_l) = \sum_{\kappa \in \mathbb{N}_0^N} \mathbf{u}_{\kappa,l}(t, x, y) \phi_{\kappa,l}(\xi_l) \approx \sum_{\kappa \in \mathcal{K}} \mathbf{u}_{\kappa,l}(t, x, y) \phi_{\kappa,l}(\xi_l), \quad (2.10)$$

for all $l \in \mathcal{L}$. The global approximation 2.4 can then be written as

$$\mathbf{u}(t, x, y, \xi) = \sum_{l \in \mathcal{L}} \mathbf{u}_l(t, x, y, \xi) \chi_l(\xi) \approx \sum_{l \in \mathcal{L}} \sum_{\kappa \in \mathcal{K}} \mathbf{u}_{\kappa,l}(t, x, y) \phi_{\kappa,l}(\xi) \chi_l(\xi), \quad (2.11)$$

where the local approximation (2.4) converges to the global solution in $L_2(\Gamma)$ as $N_\Gamma, K_\Gamma \rightarrow \infty$, cf [2].

Remark 2.2. Due to the disjoint decomposition of the random space, we may now apply the SG method from Section 2.1 on every random element D_l , $l \in \mathcal{L}$.

The expected value of \mathbf{u} is given by its moment of zeroth order. We assume that $\phi_{0,l}(\xi_l) = \prod_{n=1}^N \phi_{0,l}(\xi_l^n) = 1$ in D_l and obtain the expected value and variance using the orthonormality of the basis polynomials as

$$\begin{aligned} \mathbb{E}(\mathbf{u}) &\approx \int_{\Gamma} \sum_{l \in \mathcal{L}} \sum_{\kappa \in \mathcal{K}} \mathbf{u}_{\kappa,l} \phi_{\kappa,l} \chi_l(\xi) f_{\Xi} d\xi = \sum_{l \in \mathcal{L}} \sum_{\kappa \in \mathcal{K}} \mathbf{u}_{\kappa,l} \int_{D_l} \phi_{\kappa,l} \phi_{0,l} \mathbb{P}(\chi_l(\xi) = 1) f_{D_l} d\xi_l \\ &= \sum_{l \in \mathcal{L}} \mathbb{P}(\chi_l(\xi) = 1) \mathbf{u}_{0,l}, \end{aligned} \quad (2.12)$$

$$\text{Var}(\mathbf{u}) \approx \sum_{l \in \mathcal{L}} \left(\text{Var}(\mathbf{u}_l) + (\mathbf{u}_{0,l} - \mathbb{E}(\mathbf{u}))^2 \right) \mathbb{P}(\chi_l(\xi) = 1), \quad (2.13)$$

where the local variance $\text{Var}(\mathbf{u}_l)$ is given by

$$\text{Var}(\mathbf{u}_l) \approx \int_{D_l} \left(\sum_{\kappa \in \mathcal{K}} \mathbf{u}_{\kappa,l} \phi_{\kappa,l} \right)^2 f_{D_l} d\xi_l - \mathbf{u}_{0,l}^2 = \sum_{\kappa \in \mathcal{K} \setminus (0, \dots, 0)} \mathbf{u}_{\kappa,l}^2.$$

2.3. Hyperbolicity

The solution of the system of equations (2.1) has to fulfill certain physical properties. For example, the density or pressure should always be nonnegative for the Euler equations. This property translates into the following definition of hyperbolicity.

Definition 2.3. We call the set

$$\mathcal{R} := \left\{ \mathbf{u} \in \mathbb{R}^d \mid \alpha_1 \frac{\partial \mathbf{f}_1(\mathbf{u})}{\partial \mathbf{u}} + \alpha_2 \frac{\partial \mathbf{f}_2(\mathbf{u})}{\partial \mathbf{u}} \text{ has } d \text{ real, distinct eigenvalues } \forall \alpha_1, \alpha_2 \in \mathbb{R}, \alpha_1^2 + \alpha_2^2 = 1 \right\}$$

the **hyperbolicity set** and every solution vector $\mathbf{u} \in \mathcal{R}$ **admissible**.

Assumption 2.4. In the following we assume that the hyperbolicity set \mathcal{R} is open and convex.

Theorem 2.5. If the stochastic Galerkin polynomial (2.11) is admissible, then the SG system is hyperbolic.

Proof. The proof can be found in [39]. □

It has been shown in [9] that for non-scalar and non-symmetric models like the Euler equations, the SG system may lose its hyperbolicity and thus produce non-physical states. In the following section we want to generalize the hyperbolic slope-limiter from [27], which ensures hyperbolicity of the SG system, to high-order Runge-Kutta discontinuous Galerkin schemes.

3. Hyperbolicity-preserving discontinuous stochastic Galerkin scheme (hDSG)

3.1. The Runge–Kutta discontinuous stochastic Galerkin scheme

Our aim is to construct a numerical scheme that is high order in space, time and the uncertainty. Additionally, we want to ensure that the numerical scheme preserves hyperbolicity of the resulting SG system. We therefore start with the description of the DG spatial discretization. Similar to Section 2.2, where we subdivided the random space Γ into Multi-Elements D_l , $l \in \mathcal{L}$, we now divide the spatial domain $\mathcal{X} \subset \mathbb{R}^2$ into a uniform rectangular mesh with cells $C_{i,j} = [x_{i-\frac{1}{2}}, x_{i+\frac{1}{2}}] \times [y_{j-\frac{1}{2}}, y_{j+\frac{1}{2}}]$ and cell-widths $\Delta x := (x_{i+\frac{1}{2}} - x_{i-\frac{1}{2}})$, $\Delta y := (y_{j+\frac{1}{2}} - y_{j-\frac{1}{2}})$.

For the proof of hyperbolicity-preservation in Theorem 3.7 we do not write down the DG spatial discretization of the moment-system (2.6) but rather consider the weak formulation of (2.1) with respect to (x, y) and also ξ . Therefore, we test (2.1) with test functions $v(x, y, \xi)$ where $\text{supp}(v) \subseteq C_{i,j} \times D_l$ and obtain, after one formal integration by parts, the following weak formulation

$$\begin{aligned} \partial_t \int_{C_{i,j}} \int_{D_l} \mathbf{u} v f_{D_l} d\xi_l d(x, y) &= \int_{C_{i,j}} \int_{D_l} \left(\mathbf{f}_1(\mathbf{u}) \partial_x v + \mathbf{f}_2(\mathbf{u}) \partial_y v \right) f_{D_l} d\xi_l d(x, y) \\ &\quad - \int_{y_{j-\frac{1}{2}}}^{y_{j+\frac{1}{2}}} \int_{D_l} \left[\mathbf{f}_1(\mathbf{u}) v \right]_{x_{i-\frac{1}{2}}}^{x_{i+\frac{1}{2}}} f_{D_l} d\xi_l dy - \int_{x_{i-\frac{1}{2}}}^{x_{i+\frac{1}{2}}} \int_{D_l} \left[\mathbf{f}_2(\mathbf{u}) v \right]_{y_{j-\frac{1}{2}}}^{y_{j+\frac{1}{2}}} f_{D_l} d\xi_l dx. \end{aligned} \quad (3.1)$$

We replace each component of the solution \mathbf{u} by a piecewise-polynomial approximation, i.e., $\mathbf{u}_h|_{C_{i,j} \times D_l} \in (P^{K_{\mathcal{X}}}(C_{i,j}) \otimes P^{K_{\Gamma}}(D_l))^{\otimes d}$ for polynomial degrees $K_{\mathcal{X}}, K_{\Gamma} \in \mathbb{N}_0$. As a basis of $P^{K_{\mathcal{X}}}(C_{i,j})$ we use tensor-products of one-dimensional polynomials. Thus, we define the corresponding tensor-product index set $m \in \mathcal{M} := \{m = (m_1, m_2)^T \in \mathbb{N}_0^2 \mid m_i \leq K_{\mathcal{X}}, i = 1, 2\}$. As a basis of $P^{K_{\Gamma}}(D_l)$ we use the complete polynomial space from Section 2.1.

For ease of notation, we will drop the index h in the following and write \mathbf{u} instead of \mathbf{u}_h . The local approximation in the bases of the spaces of piecewise polynomials then reads as follows

$$\mathbf{u}_{i,j,l}(t, x, y, \xi_l) := \mathbf{u}|_{C_{i,j} \times D_l}(t, x, y, \xi_l) = \sum_{m \in \mathcal{M}} \sum_{\kappa \in \mathcal{K}} \mathbf{u}_{m,\kappa,i,j,l}(t) \varphi_{m,i,j}(x, y) \phi_{\kappa,l}(\xi_l), \quad (3.2)$$

for $(x, y) \in C_{i,j}$, $\xi_l \in D_l$. Here, $\{\phi_{\kappa,l}\}_{\kappa \in \mathcal{K}}$ are the local basis polynomials on the random element D_l and $\{\varphi_{m,i,j}\}_{m \in \mathcal{M}}$ are the basis polynomials on the physical cell $C_{i,j}$. For a simpler notation we restrict ourselves to one fixed space-stochastic cell $C_{i,j} \times D_l$ and drop the additional indices i, j and l in (3.2).

Plugging the ansatz (3.2) into the weak formulation (3.1) with test functions $v = \varphi_{\tilde{m}} \phi_{\tilde{\kappa}}$ yields

$$\sum_{m \in \mathcal{M}} \sum_{\kappa \in \mathcal{K}} \partial_t \mathbf{u}_{m,\kappa} \int_{C_{i,j}} \int_{D_l} \varphi_m \varphi_{\tilde{m}} \phi_{\kappa} \phi_{\tilde{\kappa}} f_{D_l} d\xi_l d(x, y) = \int_{C_{i,j}} \int_{D_l} \left(\mathbf{f}_1(\mathbf{u}) \phi_{\tilde{\kappa}} \partial_x \varphi_{\tilde{m}} + \mathbf{f}_2(\mathbf{u}) \phi_{\tilde{\kappa}} \partial_y \varphi_{\tilde{m}} \right) f_{D_l} d\xi_l d(x, y) \quad (3.3)$$

$$- \int_{y_{j-\frac{1}{2}}}^{y_{j+\frac{1}{2}}} \int_{D_l} \left[\mathbf{f}_1(\mathbf{u}) \varphi_{\tilde{m}} \right]_{x_{i-\frac{1}{2}}}^{x_{i+\frac{1}{2}}} \phi_{\tilde{\kappa}} f_{D_l} d\xi_l dy \quad (3.4)$$

$$- \int_{x_{i-\frac{1}{2}}}^{x_{i+\frac{1}{2}}} \int_{D_l} \left[\mathbf{f}_2(\mathbf{u}) \varphi_{\tilde{m}} \right]_{y_{j-\frac{1}{2}}}^{y_{j+\frac{1}{2}}} \phi_{\tilde{\kappa}} f_{D_l} d\xi_l dx. \quad (3.5)$$

Remark 3.1. Using the orthogonality of the local basis polynomials $\{\phi_{\kappa,l}\}_{\kappa \in \mathcal{K}}$ on the random element D_l , we would come up with the DG spatial discretization of (2.6).

To approximate the integrals in (3.3), (3.4) and (3.5) numerically, we use either Gauß-Legendre or Gauß-Lobatto quadrature rules. We denote Gauß-Legendre quadrature rules with Latin letters and Gauß-Lobatto quadrature rules with Greek letters and add additional hats to the points and weights. On the spatial cell $C_{i,j}$ we use a tensor-product of one-dimensional Gauß-Lobatto quadratures with $Q_{\mathcal{X}} + 1 = \lceil \frac{K_{\mathcal{X}}+1}{2} \rceil + 1$ points and weights, denoted by $(\hat{x}_{\alpha}, \hat{w}_{\alpha})$ and $(\hat{y}_{\beta}, \hat{w}_{\beta})$, for $\alpha, \beta = 0, \dots, Q_{\mathcal{X}}$. To approximate the (spatially) one-dimensional integrals in (3.4) and (3.5), we use Gauß-Legendre quadratures with sufficient accuracy. Let us assume that we employ Gauß-Legendre quadratures with $Q_L \in \mathbb{N}_0$ points and weights denoted by (x_p, w_p) and (y_q, w_q) , for $p, q = 0, \dots, Q_L$.

For a uniformly-distributed random variable and Legendre basis functions, we apply a Gauß-Lobatto quadrature rule on D_l with order K_{Γ} , i.e., $Q_{\Gamma} + 1$ points and weights $(\hat{\xi}_{\rho}, \hat{\omega}_{\rho})$, $\rho = 0, \dots, Q_{\Gamma}$, where $Q_{\Gamma} = \lceil \frac{K_{\Gamma}+1}{2} \rceil$. For a multi-dimensional random space $\Gamma \subset \mathbb{R}^N$ we also use tensor-product quadrature rules and introduce the multi-index set $\rho \in \mathcal{P} := \{\rho = (\rho_1, \dots, \rho_N)^T \in \mathbb{N}_0^N \mid \rho_i \leq Q_{\Gamma}, i = 1, \dots, N\}$. For other probability distributions we use the corresponding Gauß quadrature based on the orthogonal basis polynomials and weighted by the probability density function f_{D_l} . We scale the quadrature weights such that

$$\sum_{\alpha=0}^{Q_{\mathcal{X}}} \sum_{q=0}^{Q_L} \sum_{\rho \in \mathcal{P}} \hat{w}_{\alpha} w_q \hat{\omega}_{\rho} = 1, \quad \sum_{p=0}^{Q_L} \sum_{\beta=0}^{Q_{\mathcal{X}}} \sum_{\rho \in \mathcal{P}} w_p \hat{w}_{\beta} \hat{\omega}_{\rho} = 1, \quad \int_{D_l} \mathbf{g} f_{D_l} d\xi_l \approx \sum_{\rho \in \mathcal{P}} \mathbf{g}(\hat{\xi}_{\rho}) \hat{\omega}_{\rho}. \quad (3.6)$$

Remark 3.2. The Gauß-Lobatto quadrature rule includes the endpoints, i.e. cell interfaces. This property will be used in the proof of Theorem 3.7.

Since $\mathbf{u}|_{C_{i,j} \times D_l}$ is discontinuous across the physical cell interfaces $x_{i \pm \frac{1}{2}}, y_{j \pm \frac{1}{2}}$, we replace the evaluation of the flux components $\mathbf{f}_1, \mathbf{f}_2$ at these points with a numerical flux function $\hat{\mathbf{f}}_1, \hat{\mathbf{f}}_2$, (approximately) solving the corresponding Riemann problem at the interface. To this end we denote the spatial traces by

$$\begin{aligned} \mathbf{u}_{i+\frac{1}{2}}^- &:= \mathbf{u}^-(x_{i+\frac{1}{2}}, y, \xi_l) := \lim_{x \uparrow x_{i+\frac{1}{2}}} \mathbf{u}|_{C_{i,j} \times D_l}(x, y, \xi_l), \\ \mathbf{u}_{i+\frac{1}{2}}^+ &:= \mathbf{u}^+(x_{i+\frac{1}{2}}, y, \xi_l) := \lim_{x \downarrow x_{i+\frac{1}{2}}} \mathbf{u}|_{C_{i,j} \times D_l}(x, y, \xi_l), \\ \mathbf{u}_{j+\frac{1}{2}}^- &:= \mathbf{u}^-(x, y_{j+\frac{1}{2}}, \xi_l) := \lim_{y \uparrow y_{j+\frac{1}{2}}} \mathbf{u}|_{C_{i,j} \times D_l}(x, y, \xi_l), \\ \mathbf{u}_{j+\frac{1}{2}}^+ &:= \mathbf{u}^+(x, y_{j+\frac{1}{2}}, \xi_l) := \lim_{y \downarrow y_{j+\frac{1}{2}}} \mathbf{u}|_{C_{i,j} \times D_l}(x, y, \xi_l). \end{aligned}$$

For our numerical experiments in Section 4 we choose either the Lax-Friedrichs numerical flux with

$$\begin{aligned} \bullet \hat{\mathbf{f}}_1(\mathbf{u}_{i+\frac{1}{2}}^-, \mathbf{u}_{i+\frac{1}{2}}^+) &:= \frac{1}{2} \left(\mathbf{f}_1(\mathbf{u}_{i+\frac{1}{2}}^-) + \mathbf{f}_1(\mathbf{u}_{i+\frac{1}{2}}^+) - \lambda_{\max}^1(\mathbf{u}_{i+\frac{1}{2}}^+ - \mathbf{u}_{i+\frac{1}{2}}^-) \right), \\ \bullet \hat{\mathbf{f}}_2(\mathbf{u}_{j+\frac{1}{2}}^-, \mathbf{u}_{j+\frac{1}{2}}^+) &:= \frac{1}{2} \left(\mathbf{f}_2(\mathbf{u}_{j+\frac{1}{2}}^-) + \mathbf{f}_2(\mathbf{u}_{j+\frac{1}{2}}^+) - \lambda_{\max}^2(\mathbf{u}_{j+\frac{1}{2}}^+ - \mathbf{u}_{j+\frac{1}{2}}^-) \right), \end{aligned}$$

where the numerical viscosity constants $\lambda_{\max}^1, \lambda_{\max}^2$ are taken as the global estimate of the absolute value of the largest eigenvalue of $\frac{\partial \mathbf{f}_1(\mathbf{u})}{\partial \mathbf{u}}$ and $\frac{\partial \mathbf{f}_2(\mathbf{u})}{\partial \mathbf{u}}$. Alternatively, we choose the HLLC numerical flux as in [10]

$$\bullet \hat{\mathbf{f}}_1(\mathbf{u}_{i+\frac{1}{2}}^-, \mathbf{u}_{i+\frac{1}{2}}^+) := \frac{b_{i+\frac{1}{2}}^+ \mathbf{f}_1(\mathbf{u}_{i+\frac{1}{2}}^-) - b_{i+\frac{1}{2}}^- \mathbf{f}_1(\mathbf{u}_{i+\frac{1}{2}}^+)}{b_{i+\frac{1}{2}}^+ - b_{i+\frac{1}{2}}^-} + \frac{b_{i+\frac{1}{2}}^+ b_{i+\frac{1}{2}}^-}{b_{i+\frac{1}{2}}^+ - b_{i+\frac{1}{2}}^-} (\mathbf{u}_{i+\frac{1}{2}}^+ - \mathbf{u}_{i+\frac{1}{2}}^-),$$

with signal speed estimates $b_{i+\frac{1}{2}}^- := \{\lambda_{\min}^1(\bar{\mathbf{u}}_{i+\frac{1}{2}}), \lambda_{\min}^1(\mathbf{u}_{i+\frac{1}{2}}^-), 0\}$, $b_{i+\frac{1}{2}}^+ := \{\lambda_{\max}^1(\bar{\mathbf{u}}_{i+\frac{1}{2}}), \lambda_{\max}^1(\mathbf{u}_{i+\frac{1}{2}}^+), 0\}$ where $\lambda_{\min}^1(\mathbf{u}), \lambda_{\max}^1(\mathbf{u})$ are the smallest and biggest eigenvalues of $\frac{\partial \mathbf{f}_1(\mathbf{u})}{\partial \mathbf{u}}$ and $\bar{\mathbf{u}}_{i+\frac{1}{2}}$ is the corresponding Roe mean value, cf. [10]. Analogously we define

$$\bullet \hat{\mathbf{f}}_2(\mathbf{u}_{j+\frac{1}{2}}^-, \mathbf{u}_{j+\frac{1}{2}}^+) := \frac{b_{j+\frac{1}{2}}^+ \mathbf{f}_2(\mathbf{u}_{j+\frac{1}{2}}^-) - b_{j+\frac{1}{2}}^- \mathbf{f}_2(\mathbf{u}_{j+\frac{1}{2}}^+)}{b_{j+\frac{1}{2}}^+ - b_{j+\frac{1}{2}}^-} + \frac{b_{j+\frac{1}{2}}^+ b_{j+\frac{1}{2}}^-}{b_{j+\frac{1}{2}}^+ - b_{j+\frac{1}{2}}^-} (\mathbf{u}_{j+\frac{1}{2}}^+ - \mathbf{u}_{j+\frac{1}{2}}^-),$$

with signal speed estimates $b_{j+\frac{1}{2}}^- := \{\lambda_{\min}^2(\bar{\mathbf{u}}_{j+\frac{1}{2}}), \lambda_{\min}^2(\mathbf{u}_{j+\frac{1}{2}}^-), 0\}$, $b_{j+\frac{1}{2}}^+ := \{\lambda_{\max}^2(\bar{\mathbf{u}}_{j+\frac{1}{2}}), \lambda_{\max}^2(\mathbf{u}_{j+\frac{1}{2}}^+), 0\}$, where $\lambda_{\min}^2(\mathbf{u}), \lambda_{\max}^2(\mathbf{u})$ are the smallest and biggest eigenvalues of $\frac{\partial \mathbf{f}_2(\mathbf{u})}{\partial \mathbf{u}}$.

The semi-discrete system (3.3)-(3.5) can now be solved numerically by a $K_{\mathcal{X}}$ -th order SSP Runge–Kutta method, see [12, 13, 28, 29]. In writing down the method we denote by

$$L_{\Delta x, \Delta y}(\mathbf{u}(t, \cdot, \cdot)) : (P^{K_{\mathcal{X}}}(C_{i,j}) \times P^{K_{\Gamma}}(D_l))^{\otimes d} \rightarrow (P^{K_{\mathcal{X}}}(C_{i,j}) \times P^{K_{\Gamma}}(D_l))^{\otimes d}$$

the right-hand side of (3.3). Furthermore,

$$\Lambda \Pi_{\Delta x, \Delta y} : \mathbb{R}^{dN_{K_{\Gamma}}} \rightarrow \mathbb{R}^{dN_{K_{\Gamma}}}$$

is the TVBM minmod slope limiter from [8].

Remark 3.3. For our numerical example in Section 4.4 we use the Finite-Volume sub-cell limiter from [31], which proved to be more robust than the TVBM limiter.

The complete time-marching algorithm for the S -stage RKDG scheme for a given n -th time-iterate $\mathbf{u}^{(n)}$ is given in Algorithm 1.

Algorithm 1 TVBM Runge–Kutta Time-Step

- 1: Set $\mathbf{v}^{(0)} = \mathbf{u}^{(n)}$.
 - 2: **for** $s = 1, \dots, S$ **do**
 - 3: Compute $\mathbf{v}^{(s)} = \Lambda \Pi_{\Delta x, \Delta y} \left(\sum_{l=0}^{s-1} \alpha_{sl} \mathbf{w}_h^{sl} \right)$, $\mathbf{w}_h^{sl} = \mathbf{v}^{(l)} + \frac{\beta_{sl}}{\alpha_{sl}} \Delta t_n L_{\Delta x, \Delta y}(\mathbf{v}^{(l)})$.
 - 4: **end for**
 - 5: Set $\mathbf{u}^{(n+1)} = \mathbf{v}^{(S)}$.
-

Remark 3.4. The initial condition $\mathbf{v}^{(0)}$ also has to be limited by $\Lambda \Pi_{\Delta x, \Delta y}$.

The parameters α_{sl} satisfy the conditions $\alpha_{sl} \geq 0$, $\sum_{l=0}^{s-1} \alpha_{sl} = 1$ and if $\beta_{sl} \neq 0$, then $\alpha_{sl} \neq 0$ for all $s = 1, \dots, S$, $l = 0, \dots, s$.

3.2. Hyperbolicity-preservation

For the proof of Theorem 3.7 we need to consider positivity-preserving numerical fluxes as for example in [43]. For a simple definition of a positivity-preserving numerical flux let us first assume that \bar{u}_i^n is the approximation of the cell average of an exact solution $u(t, x)$ in cell $[x_{i-\frac{1}{2}}, x_{i+\frac{1}{2}}]$ at time t_n . After one time-step of forward Euler we obtain at time t_{n+1}

$$\bar{u}_i^{n+1} = \bar{u}_i^n - \frac{\Delta t}{\Delta x} \left(\hat{\mathbf{f}}_1(\bar{u}_i^n, \bar{u}_{i+1}^n) - \hat{\mathbf{f}}_1(\bar{u}_{i-1}^n, \bar{u}_i^n) \right). \quad (3.7)$$

The scheme (3.7) and the numerical flux $\hat{\mathbf{f}}_1$ are called positivity-preserving, if $\bar{u}_i^n \in \mathcal{R}$ for all i implies that $\bar{u}_i^{n+1} \in \mathcal{R}$. This is in general achieved under a suitable CFL condition. Let us assume that the numerical fluxes $\hat{\mathbf{f}}_1, \hat{\mathbf{f}}_2$ are positivity-preserving.

Assumption 3.5. The numerical fluxes $\widehat{\mathbf{f}}_1, \widehat{\mathbf{f}}_2$, are positivity-preserving under a suitable CFL condition

$$\lambda_{\max}^1 \frac{\Delta t}{\Delta x} + \lambda_{\max}^2 \frac{\Delta t}{\Delta y} \leq C,$$

where $C \in (0, 1]$.

Remark 3.6. The positivity-preserving property of the Lax-Friedrichs numerical flux has been proven in [29, 43]. For the Lax-Friedrichs numerical flux, one may choose $C = 1$, cf. [43, Remark 2.4]. In [10] it has been proven that the HLLE flux is also a positivity-preserving flux. In their numerical experiments the authors set $C = 0.5$.

Theorem 3.7. Assume that $\widehat{\mathbf{f}}_1, \widehat{\mathbf{f}}_2$, are positivity-preserving numerical fluxes and assume that at time t_n all point values satisfy $\mathbf{u}(t_n, \hat{x}_\alpha, y_q, \hat{\xi}_\rho) \in \mathcal{R}$ and $\mathbf{u}(t_n, x_p, \hat{y}_\beta, \hat{\xi}_\rho) \in \mathcal{R}$ for all cells $C_{i,j} \times D_l$. Then the $x - \xi$ cell mean

$$\bar{\mathbf{u}}_{i,j,l} := \frac{1}{\int_{C_{i,j}} \int_{D_l} 1 f_{D_l} d\xi_l d(x,y)} \int_{C_{i,j}} \int_{D_l} \mathbf{u}(t, x, y, \xi_l) f_{D_l} d\xi_l d(x,y) \quad (3.8)$$

is admissible after one forward-Euler time-step of (3.3) under the modified CFL condition

$$\lambda_{\max}^1 \frac{\Delta t}{\Delta x} + \lambda_{\max}^2 \frac{\Delta t}{\Delta y} \leq C \hat{w}_0, \quad (3.9)$$

where \hat{w}_0 is the first weight of the $(Q_{\mathcal{X}} + 1)$ -point Gauß-Lobatto quadrature.

Proof. In the weak formulation (3.1), we choose the test functions as $\varphi_{\tilde{m}} = \frac{1}{\Delta x \Delta y}$ and $\phi_{\tilde{\kappa},l} = \frac{1}{\Delta \xi}$. We get

$$\begin{aligned} \partial_t \int_{C_{i,j}} \int_{D_l} \frac{1}{\Delta x \Delta y \Delta \xi} \mathbf{u} f_{D_l} d\xi_l d(x,y) &= \int_{C_{i,j}} \int_{D_l} \left(\mathbf{f}_1(\mathbf{u}) \frac{1}{\Delta \xi} \partial_x \frac{1}{\Delta x \Delta y} + \mathbf{f}_2(\mathbf{u}) \frac{1}{\Delta \xi} \partial_y \frac{1}{\Delta x \Delta y} \right) f_{D_l} d\xi_l d(x,y) \\ &\quad - \int_{y_{j-\frac{1}{2}}}^{y_{j+\frac{1}{2}}} \int_{D_l} \frac{1}{\Delta x \Delta y \Delta \xi} \left[\mathbf{f}_1(\mathbf{u}) \right]_{x_{i-\frac{1}{2}}}^{x_{i+\frac{1}{2}}} f_{D_l} d\xi_l dy \\ &\quad - \int_{x_{i-\frac{1}{2}}}^{x_{i+\frac{1}{2}}} \int_{D_l} \frac{1}{\Delta x \Delta y \Delta \xi} \left[\mathbf{f}_2(\mathbf{u}) \right]_{y_{j-\frac{1}{2}}}^{y_{j+\frac{1}{2}}} f_{D_l} d\xi_l dx. \end{aligned}$$

The definition of the cell mean, the properties $\partial_x \frac{1}{\Delta x} = 0$, $\partial_y \frac{1}{\Delta y} = 0$ and using numerical quadrature yield

$$\begin{aligned} \partial_t \bar{\mathbf{u}}_{i,j,l} &= - \frac{1}{\Delta x} \sum_{q=0}^{Q_L} \sum_{\rho \in \mathcal{P}} \left(\mathbf{f}_1(\mathbf{u}(t, x_{i+\frac{1}{2}}, y_q, \hat{\xi}_\rho)) - \mathbf{f}_1(\mathbf{u}(t, x_{i-\frac{1}{2}}, y_q, \hat{\xi}_\rho)) \right) w_q \hat{w}_\rho \\ &\quad - \frac{1}{\Delta y} \sum_{p=0}^{Q_L} \sum_{\rho \in \mathcal{P}} \left(\mathbf{f}_2(\mathbf{u}(t, x_p, y_{j+\frac{1}{2}}, \hat{\xi}_\rho)) - \mathbf{f}_2(\mathbf{u}(t, x_p, y_{j-\frac{1}{2}}, \hat{\xi}_\rho)) \right) w_p \hat{w}_\rho. \end{aligned}$$

In order to solve the Riemann problem at the cell interfaces we replace the flux components $\mathbf{f}_i(\mathbf{u})$ by the corresponding numerical fluxes $\widehat{\mathbf{f}}_i$, $i = 1, 2$.

$$\begin{aligned} \partial_t \bar{\mathbf{u}}_{i,j,l} &= - \frac{1}{\Delta x} \sum_{q=0}^{Q_L} \sum_{\rho \in \mathcal{P}} \left(\widehat{\mathbf{f}}_1(\mathbf{u}(t, x_{i+\frac{1}{2}}^-, y_q, \hat{\xi}_\rho), \mathbf{u}(t, x_{i+\frac{1}{2}}^+, y_q, \hat{\xi}_\rho)) - \widehat{\mathbf{f}}_1(\mathbf{u}(t, x_{i-\frac{1}{2}}^-, y_q, \hat{\xi}_\rho), \mathbf{u}(t, x_{i-\frac{1}{2}}^+, y_q, \hat{\xi}_\rho)) \right) w_q \hat{w}_\rho \\ &\quad - \frac{1}{\Delta y} \sum_{p=0}^{Q_L} \sum_{\rho \in \mathcal{P}} \left(\widehat{\mathbf{f}}_2(\mathbf{u}(t, x_p, y_{j+\frac{1}{2}}^-, \hat{\xi}_\rho), \mathbf{u}(t, x_p, y_{j+\frac{1}{2}}^+, \hat{\xi}_\rho)) - \widehat{\mathbf{f}}_2(\mathbf{u}(t, x_p, y_{j-\frac{1}{2}}^-, \hat{\xi}_\rho), \mathbf{u}(t, x_p, y_{j-\frac{1}{2}}^+, \hat{\xi}_\rho)) \right) w_p \hat{w}_\rho. \end{aligned} \quad (3.10)$$

We can write the cell mean evaluated at time step t_n as

$$\bar{\mathbf{u}}_{i,j,l}^{(n)} = \sum_{p=0}^{Q_L} \sum_{\beta=0}^{Q_X} \sum_{\rho \in \mathcal{P}} \mathbf{u}(t_n, x_p, \hat{y}_\beta, \hat{\xi}_\rho) w_p \hat{w}_\beta \hat{\omega}_\rho = \sum_{\alpha=0}^{Q_X} \sum_{q=0}^{Q_L} \sum_{\rho \in \mathcal{P}} \mathbf{u}(t_n, \hat{x}_\alpha, y_q, \hat{\xi}_\rho) \hat{w}_\alpha w_q \hat{\omega}_\rho.$$

Let us define $\delta_1 := \lambda_{\max}^1 \frac{\Delta t}{\Delta x}$, $\delta_2 := \lambda_{\max}^2 \frac{\Delta t}{\Delta y}$ and $\mu := \delta_1 + \delta_2$. This allows us to write

$$\begin{aligned} \bar{\mathbf{u}}_{i,j,l}^{(n)} &= \frac{\delta_1}{\mu} \bar{\mathbf{u}}_{i,j,l}^{(n)} + \frac{\delta_2}{\mu} \bar{\mathbf{u}}_{i,j,l}^{(n)} \\ &= \frac{\delta_1}{\mu} \sum_{\alpha=0}^{Q_X} \sum_{q=0}^{Q_L} \sum_{\rho \in \mathcal{P}} \mathbf{u}(t_n, \hat{x}_\alpha, y_q, \hat{\xi}_\rho) \hat{w}_\alpha w_q \hat{\omega}_\rho + \frac{\delta_2}{\mu} \sum_{p=0}^{Q_L} \sum_{\beta=0}^{Q_X} \sum_{\rho \in \mathcal{P}} \mathbf{u}(t_n, x_p, \hat{y}_\beta, \hat{\xi}_\rho) w_p \hat{w}_\beta \hat{\omega}_\rho \\ &= \frac{\delta_1}{\mu} \sum_{\alpha=1}^{Q_X-1} \sum_{q=0}^{Q_L} \sum_{\rho \in \mathcal{P}} \mathbf{u}(t_n, \hat{x}_\alpha, y_q, \hat{\xi}_\rho) \hat{w}_\alpha w_q \hat{\omega}_\rho \\ &\quad + \frac{\delta_1}{\mu} \hat{w}_0 \sum_{q=0}^{Q_L} \sum_{\rho \in \mathcal{P}} \left(\mathbf{u}(t_n, x_{i-\frac{1}{2}}^+, y_q, \hat{\xi}_\rho) + \mathbf{u}(t_n, x_{i+\frac{1}{2}}^-, y_q, \hat{\xi}_\rho) \right) w_q \hat{\omega}_\rho, \\ &\quad + \frac{\delta_2}{\mu} \sum_{p=0}^{Q_L} \sum_{\beta=1}^{Q_X-1} \sum_{\rho \in \mathcal{P}} \mathbf{u}(t_n, x_p, \hat{y}_\beta, \hat{\xi}_\rho) w_p \hat{w}_\beta \hat{\omega}_\rho \\ &\quad + \frac{\delta_2}{\mu} \hat{w}_0 \sum_{p=0}^{Q_L} \sum_{\rho \in \mathcal{P}} \left(\mathbf{u}(t_n, x_p, y_{j-\frac{1}{2}}^+, \hat{\xi}_\rho) + \mathbf{u}(t_n, x_p, y_{j+\frac{1}{2}}^-, \hat{\xi}_\rho) \right) w_p \hat{\omega}_\rho, \end{aligned} \tag{3.11}$$

where we used the fact that $\hat{w}_0 = \hat{w}_{Q_X}$, $y_{j-\frac{1}{2}}^+ = \hat{y}_0|_{C_{i,j}}$, $y_{j+\frac{1}{2}}^- = \hat{y}_{Q_X}|_{C_{i,j}}$, $x_{i-\frac{1}{2}}^+ = \hat{x}_0|_{C_{i,j}}$, $x_{i+\frac{1}{2}}^- = \hat{x}_{Q_X}|_{C_{i,j}}$. One time-step of forward Euler of (3.10) reads as follows

$$\begin{aligned} \bar{\mathbf{u}}_{i,j,l}^{(n+1)} &= \bar{\mathbf{u}}_{i,j,l}^{(n)} \\ &\quad - \frac{\Delta t}{\Delta x} \sum_{q=0}^{Q_L} \sum_{\rho \in \mathcal{P}} \left(\hat{\mathbf{f}}_1(\mathbf{u}(t_n, x_{i+\frac{1}{2}}^-, y_q, \hat{\xi}_\rho), \mathbf{u}(t_n, x_{i+\frac{1}{2}}^+, y_q, \hat{\xi}_\rho)) - \hat{\mathbf{f}}_1(\mathbf{u}(t_n, x_{i-\frac{1}{2}}^-, y_q, \hat{\xi}_\rho), \mathbf{u}(t_n, x_{i-\frac{1}{2}}^+, y_q, \hat{\xi}_\rho)) \right) w_q \hat{\omega}_\rho \\ &\quad - \frac{\Delta t}{\Delta y} \sum_{p=0}^{Q_L} \sum_{\rho \in \mathcal{P}} \left(\hat{\mathbf{f}}_2(\mathbf{u}(t_n, x_p, y_{j+\frac{1}{2}}^-, \hat{\xi}_\rho), \mathbf{u}(t_n, x_p, y_{j+\frac{1}{2}}^+, \hat{\xi}_\rho)) - \hat{\mathbf{f}}_2(\mathbf{u}(t_n, x_p, y_{j-\frac{1}{2}}^-, \hat{\xi}_\rho), \mathbf{u}(t_n, x_p, y_{j-\frac{1}{2}}^+, \hat{\xi}_\rho)) \right) w_p \hat{\omega}_\rho. \end{aligned} \tag{3.12}$$

Using (3.11) gives

$$\begin{aligned}
\bar{\mathbf{u}}_{i,j,l}^{(n+1)} &= \frac{\delta_1}{\mu} \sum_{\alpha=1}^{Q_X-1} \sum_{q=0}^{Q_L} \sum_{\rho \in \mathcal{P}} \mathbf{u}(t_n, \hat{x}_\alpha, y_q, \hat{\xi}_\rho) \hat{w}_\alpha w_q \hat{\omega}_\rho \\
&+ \frac{\delta_1}{\mu} \hat{w}_0 \sum_{q=0}^{Q_L} \sum_{\rho \in \mathcal{P}} \left(\mathbf{u}(t_n, x_{i-\frac{1}{2}}^+, y_q, \hat{\xi}_\rho) + \mathbf{u}(t_n, x_{i+\frac{1}{2}}^-, y_q, \hat{\xi}_\rho) \right) w_q \hat{\omega}_\rho, \\
&+ \frac{\delta_2}{\mu} \sum_{p=0}^{Q_L} \sum_{\beta=1}^{Q_X-1} \sum_{\rho \in \mathcal{P}} \mathbf{u}(t_n, x_p, \hat{y}_\beta, \hat{\xi}_\rho) w_p \hat{w}_\beta \hat{\omega}_\rho \\
&+ \frac{\delta_2}{\mu} \hat{w}_0 \sum_{p=0}^{Q_L} \sum_{\rho \in \mathcal{P}} \left(\mathbf{u}(t_n, x_p, y_{j-\frac{1}{2}}^+, \hat{\xi}_\rho) + \mathbf{u}(t_n, x_p, y_{j+\frac{1}{2}}^-, \hat{\xi}_\rho) \right) w_p \hat{\omega}_\rho \\
&- \frac{\delta_1}{\lambda_{\max}^1} \sum_{q=0}^{Q_L} \sum_{\rho \in \mathcal{P}} \left(\hat{\mathbf{f}}_1(\mathbf{u}(t_n, x_{i-\frac{1}{2}}^-, y_q, \hat{\xi}_\rho), \mathbf{u}(t_n, x_{i+\frac{1}{2}}^+, y_q, \hat{\xi}_\rho)) - \hat{\mathbf{f}}_1(\mathbf{u}(t_n, x_{i-\frac{1}{2}}^-, y_q, \hat{\xi}_\rho), \mathbf{u}(t_n, x_{i-\frac{1}{2}}^+, y_q, \hat{\xi}_\rho)) \right) w_q \hat{\omega}_\rho \\
&- \frac{\delta_2}{\lambda_{\max}^2} \sum_{p=0}^{Q_L} \sum_{\rho \in \mathcal{P}} \left(\hat{\mathbf{f}}_2(\mathbf{u}(t_n, x_p, y_{j+\frac{1}{2}}^-, \hat{\xi}_\rho), \mathbf{u}(t_n, x_p, y_{j+\frac{1}{2}}^+, \hat{\xi}_\rho)) - \hat{\mathbf{f}}_2(\mathbf{u}(t_n, x_p, y_{j-\frac{1}{2}}^-, \hat{\xi}_\rho), \mathbf{u}(t_n, x_p, y_{j-\frac{1}{2}}^+, \hat{\xi}_\rho)) \right) w_p \hat{\omega}_\rho.
\end{aligned}$$

Adding and subtracting $\hat{\mathbf{f}}_1(\mathbf{u}(t_n, x_{i-\frac{1}{2}}^+, y_q, \hat{\xi}_\rho), \mathbf{u}(t_n, x_{i+\frac{1}{2}}^-, y_q, \hat{\xi}_\rho))$ and $\hat{\mathbf{f}}_2(\mathbf{u}(t_n, x_p, y_{j-\frac{1}{2}}^+, \hat{\xi}_\rho), \mathbf{u}(t_n, x_p, y_{j+\frac{1}{2}}^-, \hat{\xi}_\rho))$ yields

$$\begin{aligned}
\bar{\mathbf{u}}_{i,j,l}^{(n+1)} &= \frac{\delta_1}{\mu} \sum_{\alpha=1}^{Q_X-1} \sum_{q=0}^{Q_L} \sum_{\rho \in \mathcal{P}} \mathbf{u}(t_n, \hat{x}_\alpha, y_q, \hat{\xi}_\rho) \hat{w}_\alpha w_q \hat{\omega}_\rho + \frac{\delta_2}{\mu} \sum_{p=0}^{Q_L} \sum_{\beta=1}^{Q_X-1} \sum_{\rho \in \mathcal{P}} \mathbf{u}(t_n, x_p, \hat{y}_\beta, \hat{\xi}_\rho) w_p \hat{w}_\beta \hat{\omega}_\rho \\
&+ \frac{\delta_1}{\mu} \hat{w}_0 \sum_{q=0}^{Q_L} \sum_{\rho \in \mathcal{P}} \left(\mathbf{u}(t_n, x_{i-\frac{1}{2}}^+, y_q, \hat{\xi}_\rho) + \mathbf{u}(t_n, x_{i+\frac{1}{2}}^-, y_q, \hat{\xi}_\rho) \right) w_q \hat{\omega}_\rho, \\
&+ \frac{\delta_2}{\mu} \hat{w}_0 \sum_{p=0}^{Q_L} \sum_{\rho \in \mathcal{P}} \left(\mathbf{u}(t_n, x_p, y_{j-\frac{1}{2}}^+, \hat{\xi}_\rho) + \mathbf{u}(t_n, x_p, y_{j+\frac{1}{2}}^-, \hat{\xi}_\rho) \right) w_p \hat{\omega}_\rho \\
&- \frac{\delta_1}{\lambda_{\max}^1} \sum_{q=0}^{Q_L} \sum_{\rho \in \mathcal{P}} \left(\hat{\mathbf{f}}_1(\mathbf{u}(t_n, x_{i-\frac{1}{2}}^-, y_q, \hat{\xi}_\rho), \mathbf{u}(t_n, x_{i+\frac{1}{2}}^+, y_q, \hat{\xi}_\rho)) - \hat{\mathbf{f}}_1(\mathbf{u}(t_n, x_{i-\frac{1}{2}}^+, y_q, \hat{\xi}_\rho), \mathbf{u}(t_n, x_{i+\frac{1}{2}}^-, y_q, \hat{\xi}_\rho)) \right) w_q \hat{\omega}_\rho \\
&- \frac{\delta_1}{\lambda_{\max}^1} \sum_{q=0}^{Q_L} \sum_{\rho \in \mathcal{P}} \left(\hat{\mathbf{f}}_1(\mathbf{u}(t_n, x_{i-\frac{1}{2}}^+, y_q, \hat{\xi}_\rho), \mathbf{u}(t_n, x_{i+\frac{1}{2}}^-, y_q, \hat{\xi}_\rho)) - \hat{\mathbf{f}}_1(\mathbf{u}(t_n, x_{i-\frac{1}{2}}^-, y_q, \hat{\xi}_\rho), \mathbf{u}(t_n, x_{i-\frac{1}{2}}^+, y_q, \hat{\xi}_\rho)) \right) w_q \hat{\omega}_\rho \\
&- \frac{\delta_2}{\lambda_{\max}^2} \sum_{p=0}^{Q_L} \sum_{\rho \in \mathcal{P}} \left(\hat{\mathbf{f}}_2(\mathbf{u}(t_n, x_p, y_{j+\frac{1}{2}}^-, \hat{\xi}_\rho), \mathbf{u}(t_n, x_p, y_{j+\frac{1}{2}}^+, \hat{\xi}_\rho)) - \hat{\mathbf{f}}_2(\mathbf{u}(t_n, x_p, y_{j-\frac{1}{2}}^+, \hat{\xi}_\rho), \mathbf{u}(t_n, x_p, y_{j-\frac{1}{2}}^-, \hat{\xi}_\rho)) \right) w_p \hat{\omega}_\rho \\
&- \frac{\delta_2}{\lambda_{\max}^2} \sum_{p=0}^{Q_L} \sum_{\rho \in \mathcal{P}} \left(\hat{\mathbf{f}}_2(\mathbf{u}(t_n, x_p, y_{j-\frac{1}{2}}^+, \hat{\xi}_\rho), \mathbf{u}(t_n, x_p, y_{j-\frac{1}{2}}^-, \hat{\xi}_\rho)) - \hat{\mathbf{f}}_2(\mathbf{u}(t_n, x_p, y_{j+\frac{1}{2}}^-, \hat{\xi}_\rho), \mathbf{u}(t_n, x_p, y_{j+\frac{1}{2}}^+, \hat{\xi}_\rho)) \right) w_p \hat{\omega}_\rho.
\end{aligned}$$

If we rearrange the previous equation we obtain

$$\begin{aligned}
\bar{\mathbf{u}}_{i,j,l}^{(n+1)} = & \frac{\delta_1}{\mu} \sum_{\alpha=1}^{Q_{\mathcal{X}}-1} \sum_{q=0}^{Q_L} \sum_{\rho \in \mathcal{P}} \mathbf{u}(t_n, \hat{x}_\alpha, y_q, \hat{\xi}_\rho) \hat{w}_\alpha w_q \hat{w}_\rho + \frac{\delta_2}{\mu} \sum_{p=0}^{Q_L} \sum_{\beta=1}^{Q_{\mathcal{X}}-1} \sum_{\rho \in \mathcal{P}} \mathbf{u}(t_n, x_p, \hat{y}_\beta, \hat{\xi}_\rho) w_p \hat{w}_\beta \hat{w}_\rho \\
& + \frac{\delta_1}{\mu} \hat{w}_0 \sum_{q=0}^{Q_L} \sum_{\rho \in \mathcal{P}} w_q \hat{w}_\rho \left(\mathbf{u}(t_n, x_{i-\frac{1}{2}}^+, y_q, \hat{\xi}_\rho) \right. \\
& - \frac{\mu}{\lambda_{\max}^1 \hat{w}_0} \left(\hat{\mathbf{f}}_1(\mathbf{u}(t_n, x_{i-\frac{1}{2}}^+, y_q, \hat{\xi}_\rho), \mathbf{u}(t_n, x_{i+\frac{1}{2}}^-, y_q, \hat{\xi}_\rho)) - \hat{\mathbf{f}}_1(\mathbf{u}(t_n, x_{i-\frac{1}{2}}^-, y_q, \hat{\xi}_\rho), \mathbf{u}(t_n, x_{i-\frac{1}{2}}^+, y_q, \hat{\xi}_\rho)) \right) \\
& + \frac{\delta_1}{\mu} \hat{w}_0 \sum_{q=0}^{Q_L} \sum_{\rho \in \mathcal{P}} w_q \hat{w}_\rho \left(\mathbf{u}(t_n, x_{i+\frac{1}{2}}^-, y_q, \hat{\xi}_\rho) + \mathbf{u}(t_n, x_{i+\frac{1}{2}}^-, y_q, \hat{\xi}_\rho) \right. \\
& - \frac{\mu}{\lambda_{\max}^1 \hat{w}_0} \left(\hat{\mathbf{f}}_1(\mathbf{u}(t_n, x_{i+\frac{1}{2}}^-, y_q, \hat{\xi}_\rho), \mathbf{u}(t_n, x_{i+\frac{1}{2}}^+, y_q, \hat{\xi}_\rho)) - \hat{\mathbf{f}}_1(\mathbf{u}(t_n, x_{i-\frac{1}{2}}^+, y_q, \hat{\xi}_\rho), \mathbf{u}(t_n, x_{i+\frac{1}{2}}^-, y_q, \hat{\xi}_\rho)) \right) \\
& + \frac{\delta_2}{\mu} \hat{w}_0 \sum_{p=0}^{Q_L} \sum_{\rho \in \mathcal{P}} w_p \hat{w}_\rho \left(\mathbf{u}(t_n, x_p, y_{j-\frac{1}{2}}^+, \hat{\xi}_\rho) \right. \\
& - \frac{\mu}{\lambda_{\max}^2 \hat{w}_0} \left(\hat{\mathbf{f}}_2(\mathbf{u}(t_n, x_p, y_{j-\frac{1}{2}}^+, \hat{\xi}_\rho), \mathbf{u}(t_n, x_p, y_{j+\frac{1}{2}}^-, \hat{\xi}_\rho)) - \hat{\mathbf{f}}_2(\mathbf{u}(t_n, x_p, y_{j-\frac{1}{2}}^-, \hat{\xi}_\rho), \mathbf{u}(t_n, x_p, y_{j-\frac{1}{2}}^+, \hat{\xi}_\rho)) \right) \\
& + \frac{\delta_2}{\mu} \hat{w}_0 \sum_{p=0}^{Q_L} \sum_{\rho \in \mathcal{P}} w_p \hat{w}_\rho \left(\mathbf{u}(t_n, x_p, y_{j+\frac{1}{2}}^-, \hat{\xi}_\rho) \right. \\
& - \frac{\mu}{\lambda_{\max}^2 \hat{w}_0} \left(\hat{\mathbf{f}}_2(\mathbf{u}(t_n, x_p, y_{j+\frac{1}{2}}^-, \hat{\xi}_\rho), \mathbf{u}(t_n, x_p, y_{j+\frac{1}{2}}^+, \hat{\xi}_\rho)) - \hat{\mathbf{f}}_2(\mathbf{u}(t_n, x_p, y_{j-\frac{1}{2}}^+, \hat{\xi}_\rho), \mathbf{u}(t_n, x_p, y_{j+\frac{1}{2}}^-, \hat{\xi}_\rho)) \right) \Big).
\end{aligned} \tag{3.13}$$

Now every term of the form

$$\mathbf{u}(t_n, x_{i-\frac{1}{2}}^+, y_q, \hat{\xi}_\rho) - \frac{\mu}{\lambda_{\max}^1 \hat{w}_0} \left(\hat{\mathbf{f}}_1(\mathbf{u}(t_n, x_{i-\frac{1}{2}}^+, y_q, \hat{\xi}_\rho), \mathbf{u}(t_n, x_{i+\frac{1}{2}}^-, y_q, \hat{\xi}_\rho)) - \hat{\mathbf{f}}_1(\mathbf{u}(t_n, x_{i-\frac{1}{2}}^-, y_q, \hat{\xi}_\rho), \mathbf{u}(t_n, x_{i-\frac{1}{2}}^+, y_q, \hat{\xi}_\rho)) \right)$$

and

$$\mathbf{u}(t_n, x_p, y_{j-\frac{1}{2}}^+, \hat{\xi}_\rho) - \frac{\mu}{\lambda_{\max}^2 \hat{w}_0} \left(\hat{\mathbf{f}}_2(\mathbf{u}(t_n, x_p, y_{j-\frac{1}{2}}^+, \hat{\xi}_\rho), \mathbf{u}(t_n, x_p, y_{j+\frac{1}{2}}^-, \hat{\xi}_\rho)) - \hat{\mathbf{f}}_2(\mathbf{u}(t_n, x_p, y_{j-\frac{1}{2}}^-, \hat{\xi}_\rho), \mathbf{u}(t_n, x_p, y_{j-\frac{1}{2}}^+, \hat{\xi}_\rho)) \right)$$

is admissible under the modified CFL condition

$$\lambda_{\max}^1 \frac{\Delta t}{\Delta x} + \lambda_{\max}^2 \frac{\Delta t}{\Delta y} \leq C \hat{w}_0.$$

Hence, $\bar{\mathbf{u}}_{i,j,l}^{(n+1)}$ is a convex combination of admissible quantities in \mathcal{R} and therefore $\bar{\mathbf{u}}_{i,j,l}^{(n+1)} \in \mathcal{R}$. \square

Remark 3.1. In the one-dimensional case $\mathcal{X} \subset \mathbb{R}$, we only have to verify $\mathbf{u}(t_n, \hat{x}_\alpha, \hat{\xi}_\rho) \in \mathcal{R}$ for all cells $C_i \times D_l$ in order to apply Theorem 3.7.

3.3. Hyperbolicity limiter

To ensure that at time t_n all point values satisfy $\mathbf{u}(t_n, \hat{x}_\alpha, y_q, \hat{\xi}_\rho) \in \mathcal{R}$ and $\mathbf{u}(t_n, x_p, \hat{y}_\beta, \hat{\xi}_\rho) \in \mathcal{R}$ for each cell $C_{i,j} \times D_l$, we define the slope-limited polynomial in $C_{i,j} \times D_l$ as

$$\Lambda \Pi^\theta(\mathbf{u}_{i,j,l})(t, x, y, \xi_l) := \theta \bar{\mathbf{u}}_{i,j,l} + (1 - \theta) \mathbf{u}_{i,j,l}(t, x, y, \xi_l). \tag{3.14}$$

The variable θ limits the polynomial towards the (assumed to be) admissible cell mean.

The case $\theta = 0$ coincides with the unlimited solution and for $\theta = 1$ we have

$$\Lambda\Pi^{\theta=1}(\mathbf{u}_{i,j,l})(t, x, y, \boldsymbol{\xi}_l) = \bar{\mathbf{u}}_{i,j,l}^{(n)},$$

which is supposed to be admissible. Because of this property and since \mathcal{R} is convex, we can choose

$$\hat{\theta}_{i,j,l}(t_n) := \inf \left\{ \tilde{\theta} \in [0, 1] \mid \Lambda\Pi^{\tilde{\theta}}(\mathbf{u}_{i,j,l})(t_n, \hat{x}_\alpha, \hat{y}_q, \hat{\boldsymbol{\xi}}_\rho) \in \mathcal{R} \wedge \Lambda\Pi^{\tilde{\theta}}(\mathbf{u}_{i,j,l})(t_n, x_p, \hat{y}_\beta, \hat{\boldsymbol{\xi}}_\rho) \in \mathcal{R} \right. \\ \left. \forall \alpha, \beta, p, q = 0, \dots, Q_{\mathcal{X}}, \rho = 0, \dots, Q_{\Gamma} \right\}.$$

Due to the openness of \mathcal{R} , we need to modify θ slightly in order to avoid placing the solution onto the boundary (if the limiter was active). Therefore we use

$$\theta = \begin{cases} \hat{\theta}, & \text{if } \hat{\theta} = 0, \\ \min(\hat{\theta} + \varepsilon, 1), & \text{if } \hat{\theta} > 0, \end{cases}$$

where $0 < \varepsilon = 10^{-10}$ should be chosen small enough to ensure that the approximation quality is not influenced significantly.

Using the limited point values, we derive the updated coefficients via

$$\mathbf{u}_{m,\kappa}(t_n) = \sum_{\alpha=0}^{Q_{\mathcal{X}}} \sum_{\beta=0}^{Q_{\mathcal{X}}} \sum_{\rho \in \mathcal{P}} \Lambda\Pi^{\theta}(\mathbf{u}_{i,j,l})(t_n, \hat{x}_\alpha, \hat{y}_\beta, \hat{\boldsymbol{\xi}}_\rho) \varphi_m(\hat{x}_\alpha, \hat{y}_\beta) \phi_\kappa(\hat{\boldsymbol{\xi}}_\rho) \hat{w}_\alpha \hat{w}_\beta \hat{w}_\rho, \quad \forall m = 0, \dots, K_{\mathcal{X}}, \kappa = 0, \dots, K_{\Gamma}.$$

Note that the cell mean is preserved since

$$\begin{aligned} & \sum_{\alpha=0}^{Q_{\mathcal{X}}} \sum_{\beta=0}^{Q_{\mathcal{X}}} \sum_{\rho \in \mathcal{P}} \Lambda\Pi^{\theta}(\mathbf{u}_{i,j,l})(t_n, \hat{x}_\alpha, \hat{y}_\beta, \hat{\boldsymbol{\xi}}_\rho) \hat{w}_\alpha \hat{w}_\beta \hat{w}_\rho \\ &= \theta \bar{\mathbf{u}}_{i,j,l}^{(n)} \sum_{\alpha=0}^{Q_{\mathcal{X}}} \sum_{\beta=0}^{Q_{\mathcal{X}}} \sum_{\rho \in \mathcal{P}} \hat{w}_\alpha \hat{w}_\beta \hat{w}_\rho + (1 - \theta) \sum_{\alpha=0}^{Q_{\mathcal{X}}} \sum_{\beta=0}^{Q_{\mathcal{X}}} \sum_{\rho \in \mathcal{P}} \mathbf{u}(t_n, \hat{x}_\alpha, \hat{y}_\beta, \hat{\boldsymbol{\xi}}_\rho) \hat{w}_\alpha \hat{w}_\beta \hat{w}_\rho \\ &= \bar{\mathbf{u}}_{i,j,l}^{(n)}. \end{aligned}$$

Remark 3.2. In the following we will again abuse notation and write $\Lambda\Pi^{\theta}(\mathbf{u})$ for the piecewise polynomial \mathbf{u} instead of the local polynomials $\mathbf{u}_{i,j,l}$. By this we mean the application of the hyperbolicity limiter on each cell $C_{i,j} \times D_l$ separately where we obtain independent values of the limiter variable θ .

A complete Runge–Kutta time-step using the hyperbolicity-preserving limiter is shown in Algorithm 2.

Algorithm 2 TVBM Runge–Kutta time-step with hyperbolic limiter

- 1: Set $\mathbf{v}^{(0)} = \mathbf{u}^{(n)}$.
 - 2: **for** $s = 1, \dots, S$ **do**
 - 3: Compute $\mathbf{v}^{(s)} = \Lambda\Pi_{\Delta x, \Delta y} \left(\sum_{l=0}^{s-1} \alpha_{sl} \mathbf{w}_h^{sl} \right)$, $\mathbf{w}_h^{sl} = \mathbf{v}^{(l)} + \frac{\beta_{sl}}{\alpha_{sl}} \Delta t_n L_{\Delta x, \Delta y}(\mathbf{v}^{(l)})$.
 - 4: Compute $\mathbf{v}^{(s)} = \Lambda\Pi^{\theta}(\mathbf{v}^{(s)})$.
 - 5: **end for**
 - 6: Set $\mathbf{u}^{(n+1)} = \mathbf{v}^{(S)}$
-

Remark 3.8. The initial condition \mathbf{u}^0 also has to be limited by both limiters $\Lambda\Pi_{\Delta x, \Delta y}$ and $\Lambda\Pi^{\theta}$.

3.3.1. Calculations for the Euler equation

The two-dimensional compressible Euler equations for the flow of an ideal gas are given by

$$\left. \begin{aligned} \partial_t \rho + \partial_x m_1 + \partial_y m_2 &= 0, \\ \partial_t m_1 + \partial_x \left(\frac{m_1^2}{\rho} + p \right) + \partial_y \left(\frac{m_1 m_2}{\rho} \right) &= 0, \\ \partial_t m_2 + \partial_x \left(\frac{m_1 m_2}{\rho} \right) + \partial_y \left(\frac{m_2^2}{\rho} + p \right) &= 0, \\ \partial_t E + \partial_x \left((E + p) \frac{m_1}{\rho} \right) + \partial_y \left((E + p) \frac{m_2}{\rho} \right) &= 0, \end{aligned} \right\} \quad (3.15)$$

where ρ describes the mass density, m_1 and m_2 the momentum in x and y direction and E the energy of the gas. The three equations model the conservation of mass, momentum and energy. The pressure p reads

$$p = (\gamma - 1) \left(E - \frac{1}{2} \frac{(m_1^2 + m_2^2)}{\rho} \right),$$

with the adiabatic constant $\gamma > 1$. The hyperbolicity set is given by

$$\mathcal{R} = \left\{ \mathbf{u} = \begin{pmatrix} \rho \\ m_1 \\ m_2 \\ E \end{pmatrix} \left| \rho > 0, p = (\gamma - 1) \left(E - \frac{1}{2} \frac{(m_1^2 + m_2^2)}{\rho} \right) > 0 \right. \right\}.$$

Lemma 3.9. *Let $\tilde{\mathbf{u}} = (\tilde{\rho}, \tilde{m}_1, \tilde{m}_2, \tilde{E})^T \in \mathcal{R}$ and $\mathbf{u} = (\rho, m_1, m_2, E)^T \in \mathbb{R}^4$ be arbitrary. Then the solution of the hyperbolicity limiter problem*

$$\begin{aligned} \min \quad & \theta \\ \text{s.t.} \quad & \theta \in [0, 1] \\ & \theta \tilde{\mathbf{u}} + (1 - \theta) \mathbf{u} \in \mathcal{R} \end{aligned}$$

for the two-dimensional Euler equations has the solution

$$\begin{aligned} \theta^* &= \max(h(\theta_1), h(\theta_{2+}), h(\theta_{2-})), \\ h(x) &= x \mathbb{1}_{[0,1]}(x), \\ \theta_1 &= \frac{\rho}{\rho - \tilde{\rho}}, \\ \theta_{2\pm} &= \frac{\rho \tilde{E} - 2\rho E + \tilde{\rho} E - m_1 \tilde{m}_1 - m_2 \tilde{m}_2 \pm \sqrt{\tilde{\theta}}}{m_1^2 - 2m_1 \tilde{m}_1 + m_2^2 - 2m_2 \tilde{m}_2 + \tilde{m}_1^2 + \tilde{m}_2^2 - 2\rho E + 2\rho \tilde{E} + 2\tilde{\rho} E - 2\tilde{\rho} \tilde{E}}, \end{aligned} \quad (3.16)$$

where

$$\begin{aligned} \tilde{\theta} &= \rho^2 \tilde{E}^2 - 2\rho \tilde{\rho} E \tilde{E} + 2\rho E \tilde{m}_1^2 + 2\rho E \tilde{m}_2^2 - 2\rho \tilde{E} m_1 \tilde{m}_1 - 2\rho \tilde{E} m_2 \tilde{m}_2 \\ &\quad + \tilde{\rho}^2 E^2 - 2\tilde{\rho} E m_1 \tilde{m}_1 - 2\tilde{\rho} E m_2 \tilde{m}_2 + 2\tilde{\rho} \tilde{E} m_1^2 + 2\tilde{\rho} \tilde{E} m_2^2 - m_1^2 \tilde{m}_2^2 + 2m_1 m_2 \tilde{m}_1 \tilde{m}_2 - m_2^2 \tilde{m}_1^2. \end{aligned}$$

Proof. We derive the values of the limiter variable θ , for which the expression $\theta \tilde{\mathbf{u}} + (1 - \theta) \mathbf{u}$ is in the hyperbolicity set \mathcal{R} . In order to have a positive density we require

$$\theta \tilde{\rho} + (1 - \theta) \rho > 0,$$

yielding

$$\theta < \frac{\rho}{\rho - \tilde{\rho}} = \theta_1,$$

if $\tilde{\rho} \neq \rho$. Otherwise, we have $\rho = \tilde{\rho} > 0$ and set $\theta_1 = 0$. Analogously, we calculate the pressure term and check it for positivity

$$\frac{p}{\gamma - 1} = \theta \tilde{E} + (1 - \theta)E - \frac{1}{2} \frac{\left((\theta \tilde{m}_1 + (1 - \theta)m_1)^2 + (\theta \tilde{m}_2 + (1 - \theta)m_2)^2 \right)}{\theta \tilde{\rho} + (1 - \theta)\rho} \stackrel{!}{>} 0.$$

Since the density is supposed to be positive we can multiply it to the above equation

$$\frac{p(\theta \tilde{\rho} + (1 - \theta)\rho)}{\gamma - 1} = (\theta \tilde{E} + (1 - \theta)E)(\theta \tilde{\rho} + (1 - \theta)\rho) - \frac{1}{2} \left((\theta \tilde{m}_1 + (1 - \theta)m_1)^2 + (\theta \tilde{m}_2 + (1 - \theta)m_2)^2 \right) \stackrel{!}{>} 0.$$

Writing this inequality as a polynomial in θ we obtain

$$\begin{aligned} & \left((E - \tilde{E})(\rho - \tilde{\rho}) - \frac{1}{2}(m_1 - \tilde{m}_1)^2 - \frac{1}{2}(m_2 - \tilde{m}_2)^2 \right) \theta^2 \\ & + \left(m_1(m_1 - \tilde{m}_1) + m_2(m_2 - \tilde{m}_2) - \rho(E - \tilde{E}) - E(\rho - \tilde{\rho}) \right) \theta \\ & + E\rho - \frac{m_1^2}{2} - \frac{m_2^2}{2} \stackrel{!}{>} 0. \end{aligned}$$

The corresponding equality has the roots θ_{2+} and θ_{2-} . Combining these results with $\theta \in [0, 1]$, we end up with (3.16). \square

Remark 3.10. In the previous lemma, the quantity $\tilde{\mathbf{u}}$ plays the role of the cell mean $\bar{\mathbf{u}}_{i,j,l}$ in Theorem 3.7, whereas \mathbf{u} is given by the point values $\mathbf{u}(t, \hat{x}_\alpha, y_q, \hat{\xi}_\rho)$ and $\mathbf{u}(t, x_p, \hat{y}_\beta, \hat{\xi}_\rho)$.

4. Numerical Results

In the following numerical experiments we analyze the hyperbolicity-preserving discontinuous stochastic Galerkin (hDSG) method for different problems of the Euler equations. In Section 4.1 we apply it to a smooth solution and examine its convergence. In Section 4.2 we compare the performance of our scheme to the non-intrusive Stochastic Collocation method. We evaluate both methods for a smooth solution which depends on three random variables. Finally, in Section 4.3 and Section 4.4, we apply the hDSG method to a one- and two-dimensional Riemann problem and examine the behavior of the hyperbolicity-preserving limiter. When we employ the Multi-Element (ME) ansatz from Section 2.2, we call our method ME-hDSG.

As a numerical solver for the SG system we use a modified version of the Runge–Kutta discontinuous Galerkin solver Flexi [14] with a SSP-RK time-discretization of order four. We set the CFL-number from Assumption 3.5 to $C = 0.45$. In the following numerical examples we measure the error in mean and variance at time $t = T$ in the $L_1(\mathcal{X})$ - or $L_2(\mathcal{X})$ -norm which we approximate by a tensor product Gauß quadrature rule with 15 points (in one dimension) in every physical cell and 20 points (in one dimension) in every Multi-Element. We denote the number of spatial cells by $N_{\mathcal{X}}$ and the number of MEs by N_{Γ} .

4.1. Convergence tests

This example is devoted to the convergence of the hDSG method for smooth solutions of the Euler equations. We let the spatial domain $\mathcal{X} = [0, 1]^2$, where we use periodic boundary conditions and set the adiabatic constant to $\gamma = 1.4$. As numerical flux we use Lax-Friedrichs. To obtain an analytical solution of the Euler

equations, we consider the method of manufactured solutions. To this end we introduce an additional source term S in (3.15), where

$$S(t, x, y, \xi) := \begin{pmatrix} \partial_t \rho + \partial_x m_1 + \partial_y m_2 \\ \partial_t m_1 + \partial_x \left(\frac{m_1^2}{\rho} + p \right) + \partial_y \left(\frac{m_1 m_2}{\rho} \right) \\ \partial_t m_2 + \partial_x \left(\frac{m_1 m_2}{\rho} \right) + \partial_y \left(\frac{m_2^2}{\rho} + p \right) \\ \partial_t E + \partial_x \left((E + p) \frac{m_1}{\rho} \right) + \partial_y \left((E + p) \frac{m_2}{\rho} \right) \end{pmatrix}. \quad (4.1)$$

This additional source term allows us to consider the following analytical solution of the Euler equations

$$\mathbf{u}(t, x, y, \xi_1, \xi_2, \xi_3) = \begin{pmatrix} \rho(t, x, y, \xi_1, \xi_2, \xi_3) \\ m_1(t, x, y, \xi_1, \xi_2, \xi_3) \\ m_2(t, x, y, \xi_1, \xi_2, \xi_3) \\ E(t, x, y, \xi_1, \xi_2, \xi_3) \end{pmatrix} = \begin{pmatrix} \xi_3 + \xi_2 \cos(2\pi(x - \xi_1 t)) \\ \xi_3 + \xi_2 \cos(2\pi(x - \xi_1 t)) \\ 0 \\ (\xi_3 + \xi_2 \cos(2\pi(x - \xi_1 t)))^2 \end{pmatrix}, \quad (4.2)$$

with uniformly distributed random variables $\xi_1 \sim \mathcal{U}(0.1, 1)$, $\xi_2 \sim \mathcal{U}(0.1, 0.3)$ and $\xi_3 \sim \mathcal{U}(1.8, 2.5)$.

4.1.1. Euler Equations: smooth solution, spatial refinement

As a first benchmark example we consider a refinement of the spatial domain \mathcal{X} for a SG polynomial degree of $K_\Gamma = 10$ and one Multi-Element, i.e. $N_\Gamma = 1$, as well as DG polynomial degrees of one and three. We choose the following analytical function

$$\mathbf{u}(t, x, y, \xi_1) = \begin{pmatrix} \rho(t, x, y, \xi_1) \\ m_1(t, x, y, \xi_1) \\ m_2(t, x, y, \xi_1) \\ E(t, x, y, \xi_1) \end{pmatrix} = \begin{pmatrix} 2 + 0.1(2\pi(x - \xi_1 t)) \\ 2 + 0.1 \cos(2\pi(x - \xi_1 t)) \\ 0 \\ (2 + 0.1 \cos(2\pi(x - \xi_1 t)))^2 \end{pmatrix}, \quad (4.3)$$

where $\xi_1 \sim \mathcal{U}(0.1, 1)$. We compute the numerical approximation of (4.3) up to $T = 1$. Table 1 displays the error in mean and variance of the density.

The error is clearly dominated by the spatial error as the resolution in the stochastic space is sufficiently high. Thus, it converges with the rate of the DG method, which is $(K_\mathcal{X} + 1)/2$ in two spatial dimensions.

hDSG, $K_\mathcal{X} = 1$					hDSG, $K_\mathcal{X} = 3$				
$N_\mathcal{X}$	L_2 -Mean	eoc	L_2 -Variance	eoc	$N_\mathcal{X}$	L_2 -Mean	eoc	L_2 -Variance	eoc
4	2.7033e-02	-	5.9515e-02	-	4	9.6072e-04	-	3.4636e-03	-
16	6.7904e-03	1.00	1.0958e-02	1.22	16	4.1815e-05	2.26	1.0036e-04	2.55
64	1.1669e-03	1.27	2.466e-03	1.08	64	1.7619e-06	2.28	4.3666e-06	2.26
256	1.6904e-04	1.39	3.8439e-04	1.34	256	7.1412e-08	2.31	3.9645e-07	1.73
1024	2.4801e-05	1.38	6.967e-05	1.23	1024	2.9046e-09	2.31	1.7748e-08	2.24
4096	4.2716e-06	1.27	1.5161e-05	1.10	4096	1.6708e-10	2.06	9.6501e-10	2.10

Table 1: L_2 -errors and experimental order of convergence (eoc) for the Euler equations (density) with $K_\Gamma = 10$, $N_\Gamma = 1$, for DG polynomial degrees $K_\mathcal{X} = 1, 3$. Example 4.1.1.

4.1.2. Euler Equations: smooth solution, stochastic refinement

As next numerical example we consider a stochastic refinement, where we increase the SG polynomial degree K_Γ . We consider the same analytical function (4.3) from the previous numerical experiment. In Table 2 we show a K_Γ -refinement for one random element, i.e. $N_\Gamma = 1$. Here, the physical mesh consists of $N_\mathcal{X} = 400$ cells and a DG polynomial degree of six. For the smooth solution (4.3) we observe that the error exhibits the expected spectral convergence when we increase the SG polynomial degree.

hDSG		
K_Γ	L_2 -Mean	L_2 -Variance
1	6.7406e-06	1.3562e-05
2	3.1228e-06	8.5896e-06
3	1.6532e-06	4.5845e-06
4	5.5879e-07	1.6006e-06
5	1.2829e-07	4.3977e-07
6	2.1531e-08	8.7639e-08
7	2.7923e-09	1.2051e-08
8	2.9392e-10	1.4562e-09
9	3.5925e-11	1.131e-10
10	2.4548e-11	4.7307e-11

Table 2: L_2 -errors for the Euler equations (density) with $N_\Gamma = 1$, $N_\mathcal{X} = 400$ for DG polynomial degree $K_\mathcal{X} = 6$. Example 4.1.2.

4.2. Comparison with Stochastic Collocation method

In this section we compare the hDSG-method with a common non-intrusive method, namely the Stochastic Collocation (SC) method as described in [40]. When we use SC in combination with the ME scheme from Section 2.2, we call this method ME-SC. For the collocation points in a multi-dimensional random space Γ we use tensor-products of one-dimensional Gauß-Legendre quadrature points. The number of collocation points in one dimension is always $K_\Gamma + 1$.

To compare both methods, we measure the total elapsed time (including post-processing for SC) on a workstation equipped with an AMD Ryzen ThreadRipper 2950x processor with sixteen kernels and 128 GB RAM. As a deterministic solver for the SC method we use the standard version of Flexi [14]. Both methods are parallelized using Open MPI and we measure the total elapsed time on sixteen kernels. In the following we denote the total elapsed time by wall time.

As a benchmark solution we refer to the analytical solution (4.2), which is computed up to $T = 1$ and we successively increase the number of random variables starting from ξ_1 while fixing $\xi_2 = 0.1$, $\xi_3 = 2$ and so on. The number of physical cells is always $N_\mathcal{X} = 400$ and the DG polynomial degree is six. As numerical flux we choose Lax-Friedrichs.

4.2.1. Comparison with SC: K_Γ -refinement

In this example we consider a global K_Γ -refinement for one fixed ME, i.e. $N_\Gamma = 1$. In Figure 1 and Tables 3, 4, 5 we compare the error vs. wall time for the hDSG and the SC method in one, two and three random dimensions. In all three cases the hDSG method yields a smaller absolute error for the same number of degrees of freedoms, however, only in the one-dimensional case the hDSG scheme proves to be more efficient (in terms of error vs. wall time) than the SC method.

4.2.2. Comparison with SC: ME-refinement

In this numerical experiment we compare error vs. wall time for the ME-hDSG and ME-SC methods, while increasing the number of MEs. For both methods we consider a linear interpolation, i.e. $K_\Gamma = 1$. Again, Figure 2 and Tables 6, 7, 8 show the error vs. wall time for both methods. Similar to the K_Γ -refinement in Section 4.2.1, we observe for a one-dimensional random space Γ , that ME-hDSG is clearly more efficient than the ME-SC method. In the two-dimensional case and a small number of MEs we deduce similar results. However, for three random dimensions, ME-hDSG stands no chance against the ME-SC method in terms of efficiency. This is exactly the behavior that we expect from hDSG, because computing the orthogonal

hDSG, $N = 1$				SC, $N = 1$			
K_Γ	L_2 -Mean	L_2 -Variance	wall time [s]	K_Γ	L_2 -Mean	L_2 -Variance	wall time [s]
1	6.7406e-06	1.3562e-05	6.0	1	4.5363e-01	7.9044e-02	7.0
2	3.1228e-06	8.5896e-06	6.48	2	8.7027e-02	0.044842	6.0
3	1.6532e-06	4.5845e-06	7.88	3	6.4479e-03	1.8557e-02	6.0
4	5.5879e-07	1.6006e-06	9.70	4	2.4543e-04	3.371e-03	11.0
5	1.2829e-07	4.3977e-07	10.58	5	5.6894e-06	3.4898e-04	12.0
6	2.1531e-08	8.7639e-08	12.83	6	8.8712e-08	2.3519e-05	11.0
7	2.7923e-09	1.2051e-08	14.75	7	1.1123e-09	1.1181e-06	16.0
8	2.9392e-10	1.4562e-09	18.16	8	1.6271e-10	3.96e-08	17.0
9	3.5925e-11	1.131e-10	20.91	9	1.6612e-10	1.0709e-09	16.0
10	2.4548e-11	4.7307e-11	24.85	10	1.661e-10	4.546e-11	16.0

Table 3: L_2 -errors and wall time for the Euler equations (density) for hDSG and SC method in one random dimension. Example 4.2.1.

hDSG, $N = 2$				SC, $N = 2$			
K_Γ	L_2 -Mean	L_2 -Variance	wall time [s]	K_Γ	L_2 -Mean	L_2 -Variance	wall time [s]
1	1.2374e-04	2.5015e-04	79.67	1	4.5363e-01	8.5711e-02	9.0
2	6.041e-05	0.00018524	93.53	2	8.7027e-02	4.8613e-02	15.0
3	3.5254e-05	0.00012008	121.93	3	6.4479e-03	2.0116e-02	20.0
4	1.4209e-05	5.7537e-05	172.90	4	2.4543e-04	3.6523e-03	30.0
5	5.2814e-06	2.1894e-05	220.53	5	5.6894e-06	3.7807e-04	45.0
6	1.5886e-06	6.3609e-06	336.04	6	8.8714e-08	2.5479e-05	60.0
7	3.5052e-07	1.4504e-06	467.0	7	1.1108e-09	1.2113e-06	81.0
8	5.8279e-08	2.4925e-07	700.04	8	1.6736e-10	4.2899e-08	100.0

Table 4: L_2 -errors and wall time for the Euler equations (density) for hDSG and SC method in two random dimensions. Example 4.2.1.

hDSG, $N = 3$				SC, $N = 3$			
K_Γ	L_2 -Mean	L_2 -Variance	wall time [s]	K_Γ	L_2 -Mean	L_2 -Variance	wall time [s]
1	1.1315e-03	3.51281e-03	1844.0	1	4.5363e-01	2.4904e-01	86.0
2	2.192e-04	8.2764e-04	2722.0	2	8.7027e-02	4.8613e-02	96.0
3	5.3598e-05	2.4934e-04	5406.0	3	6.4479e-03	2.0116e-02	126.0
4	1.2283e-05	5.4753e-05	14583.0	4	2.4543e-04	3.6523e-03	182.0

Table 5: L_2 -errors and wall time for the Euler equations (density) for hDSG and SC method in three random dimensions. Example 4.2.1.

projection of the fluxes in (2.6) becomes more and more expensive when we increase the number of random dimensions. Hence, for a one and maybe a two-dimensional random space, the hDSG method yields an efficiency gain compared to SC and is not competitive beyond two dimensions.

4.3. Uncertain Sod Shock Test

In this numerical test we study the behavior of the hyperbolicity limiter $\Lambda\Pi^\theta$ when it is applied to the one-dimensional uncertain Sod shock problem from [25, 27]. We consider an uncertain position of the initial

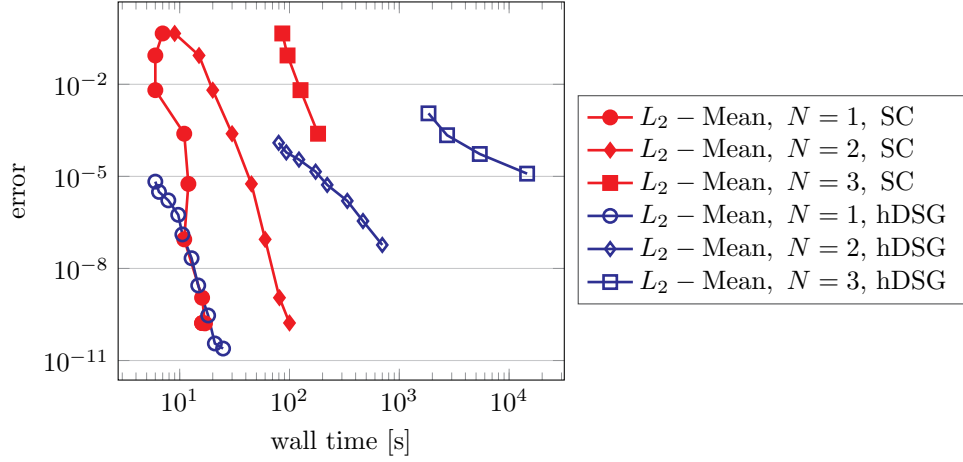


Figure 1: L_2 -errors and wall time for the Euler equations (density) for hDSG and SC method. Example 4.2.1.

ME-hDSG, $N = 1$				ME-SC, $N = 1$			
N_Γ	L_2 -Mean	L_2 -Variance	wall time [s]	N_Γ	L_2 -Mean	L_2 -Variance	wall time [s]
1	6.7125e-06	1.2071e-05	3.71	1	8.7027e-02	4.4842e-02	6.0
2	1.3863e-06	4.3691e-06	7.23	2	1.0882e-03	8.3017e-02	12.0
3	3.5026e-07	1.162e-06	11.42	3	1.8291e-04	4.2943e-04	11.0
4	1.2083e-07	4.3255e-07	14.36	4	5.4915e-05	1.0471e-04	17.0
5	5.1526e-08	1.7694e-07	19.85	5	2.1967e-05	3.859e-05	17.0
6	2.5395e-08	8.9625e-08	26.79	6	1.046e-05	1.7628e-05	22.0
7	1.3884e-08	4.8357e-08	28.32	7	5.6031e-06	9.2177e-06	27.0
8	8.2032e-09	2.9729e-08	28.98	8	3.2683e-06	5.295e-06	27.0
9	5.1462e-09	1.8097e-08	46.52	9	2.0335e-06	3.2607e-06	31.0
10	3.3861e-09	1.1955e-08	51.49	10	1.3309e-06	2.1186e-06	32.0

Table 6: L_2 -errors and wall time for the Euler equations (density) for ME-hDSG and ME-SC method in one random dimension. Example 4.2.2.

ME-hDSG, $N = 2$				ME-SC, $N = 2$			
N_Γ	L_2 -Mean	L_2 -Variance	wall time [s]	N_Γ	L_2 -Mean	L_2 -Variance	wall time [s]
1	1.2374e-04	2.5016e-04	33.26	1	8.7027e-02	4.8613e-02	15.0
4	5.7001e-05	2.9659e-04	134.32	4	1.0882e-03	8.9915e-03	30.0
9	1.6892e-05	1.1411e-04	432.19	9	1.8291e-04	4.6488e-04	60.0
16	6.1867e-06	4.6866e-05	526.07	16	5.4915e-05	1.1334e-04	101.0

Table 7: L_2 -errors and wall time for the Euler equations (density) for ME-hDSG and ME-SC method in two random dimensions. Example 4.2.2.

ME-hDSG, $N = 3$				ME-SC, $N = 3$			
N_Γ	L_2 -Mean	L_2 -Variance	wall time [s]	N_Γ	L_2 -Mean	L_2 -Variance	wall time [s]
1	1.1316e-03	3.5136e-03	239.63	1	8.7027e-02	4.8613e-02	98.0
8	1.5013e-04	7.9673e-04	1799.0	8	1.0882e-03	8.9915e-03	183.0
27	3.5281e-05	2.3186e-04	10432.13	27	1.8291e-04	4.6488e-04	414.0

Table 8: L_2 -errors and wall time for the Euler equations (density) for ME-hDSG and ME-SC method in three random dimensions. Example 4.2.2.

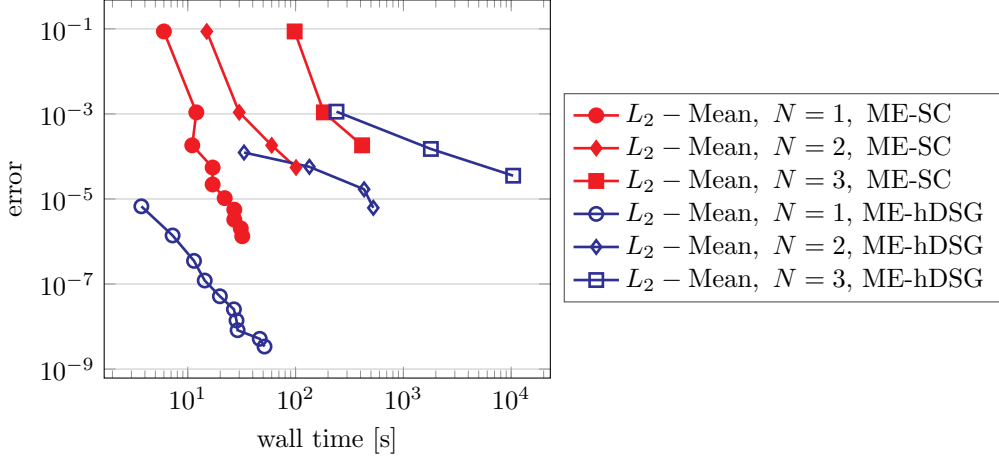


Figure 2: L_2 -errors and wall time for the Euler equations (density) for ME-hDSG and ME-SC method. Example 4.2.2

discontinuity, i.e., we have the following set of initial conditions

$$\left. \begin{aligned} \rho(t=0, x, \xi) &= \begin{cases} 1, & x < 0.5 + 0.05\xi, \\ 0.125, & x \geq 0.5 + 0.05\xi, \end{cases} \\ m(t=0, x, \xi) &= 0, \\ E(t=0, x, \xi) &= \begin{cases} 2.5, & x < 0.5 + 0.05\xi, \\ 0.25, & x \geq 0.5 + 0.05\xi, \end{cases} \end{aligned} \right\} \quad (4.4)$$

where $\xi \sim \mathcal{U}(-1, 1)$. The numerical solution is computed up to $T = 0.2$ and we define the spatial domain as $\mathcal{X} = [0, 1]$. At the boundary we prescribe exact boundary conditions. We choose the Lax-Friedrichs numerical flux and the TVBM minmod limiter from [8] as spatial limiter $\Lambda \Pi_{\Delta x, \Delta y}$.

We divide \mathcal{X} into 500 cells, set the DG polynomial degree to three and consider the hDSG and ME-hDSG method. For the hDSG scheme we use a truncation order of $K_\Gamma = 10$ and for ME-hDSG we consider $N_\Gamma = 10$ random elements and a linear approximation, i.e. $K_\Gamma = 1$. The number of quadrature nodes is set to $Q_\Gamma = 20$ and both methods are compared to a Monte Carlo simulation using an exact Riemann solver [4] with 200 000 samples.

In Figure 3 we compare mean and variance obtained by the hDSG and ME-hDSG methods against the “exact” solution given by Monte Carlo sampling. The expected value in Figure 3a and Figure 3b indicate a good agreement between Monte Carlo, hDSG and ME-hDSG. However, for the hDSG method we can see in Figure 3b and Figure 3d, especially around the shock at $x \approx 0.8$, that the hDSG solution exhibits $(K_\Gamma + 1 = 11)$ small shocks, which has also been observed for example in [9]. Because of the discontinuities in ξ , the plain hDSG approach suffers from Gibbs’ oscillations and hence using a piecewise linear interpolation, as in the Multi-Element approach, yields a far better resolution of the mean and variance compared to the plain hDSG approach.

Spurious oscillations for the hDSG method can also be observed in the $x - \xi$ -diagram in Figure 4, especially in the vicinity of the shock-curve around $x \approx 0.8$. Furthermore, the influence of the $x - \xi$ discontinuities can be seen in Table 9, where we show the error in mean and variance between the hDSG-, ME-hDSG-approximation and the Monte Carlo solution. We deduce that the error for the hDSG-approach quickly starts to stagnate, whereas the error for the Multi-Element approach is still decreasing. However, for all three methods the computed order of convergence in this example is smaller than one which is due to the discontinuities in ξ .

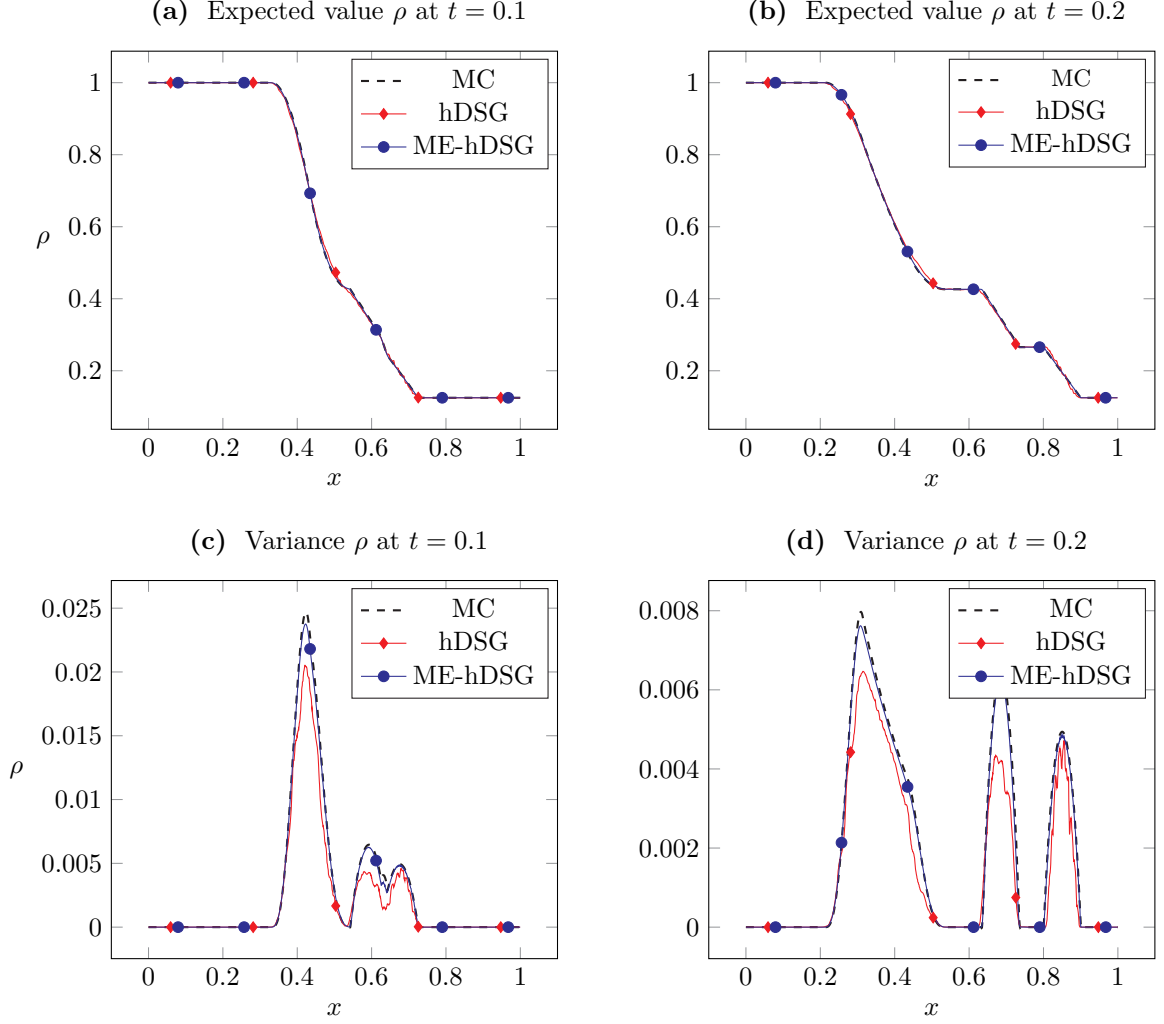


Figure 3: Euler equations with initial state (4.4), $N_{\mathcal{X}} = 500$ and DG polynomial degree $K_{\mathcal{X}} = 3$. For hDSG, $K_{\Gamma} = 10$ and for ME-hDSG $K_{\Gamma} = 1$, $N_{\Gamma} = 10$. Example 4.3.

In Figure 5 we plot the values of the limiter variable θ for the hDSG and the ME-hDSG method. In Figure 5a we can see that the limiter clearly follows the discontinuity in x . For the ME-hDSG scheme we plot the maximum value of θ over all time-steps, random and physical cells in Figure 5b. We observe that the limiter is only active for the initial condition. Afterwards, the stochastic Galerkin solution does not leave the hyperbolicity set which illustrates the strength of the Multi-Element approach. The superiority of the ME-hDSG is finally demonstrated in Table 10. Here, we display the percentage of limited cells for both methods compared to all space-time-stochastic cells. The percentage of limited cells for ME-hDSG is one order of magnitude lower than for the hDSG method.

4.4. Double Mach Reflection with Uncertain Angle

As a final numerical test for the hyperbolicity-preserving limiter, we consider the Double Mach Reflection test case suggested by Woodward and Colella [38]. It consists of a Mach 10 shock wave that hits a ramp which is inclined by 30 degrees. The Double Mach reflection poses a very challenging problem for the hDSG method because the solution is very likely to leave the hyperbolicity set due to the high jump in pressure.

ME-hDSG, $K_\Gamma = 0$					ME-hDSG, $K_\Gamma = 1$				
N_Γ	L_1 -Mean	eoc	L_1 -Variance	eoc	N_Γ	L_1 -Mean	eoc	L_1 -Variance	eoc
2	0.0086	–	8.8862e-04	–	2	0.0054	–	5.5152e-04	–
4	0.0043	1.02	4.3359e-04	1.04	4	0.0027	0.98	2.8091e-04	0.97
8	0.0021	0.99	2.2043e-04	0.98	8	0.0016	0.75	1.6526e-04	0.77
16	0.0012	0.83	1.2997e-04	0.76	16	0.0011	0.55	1.1586e-04	0.51

hDSG				
K_Γ	L_1 -Mean	eoc	L_1 -Variance	eoc
2	0.0075	–	7.3846e-04	–
4	0.0049	0.61	5.7026e-04	0.37
8	0.0038	0.37	4.4814e-04	0.35
16	0.0037	0.02	4.3632e-04	0.04

Table 9: L_1 -errors and experimental order of convergence (eoc) for the Euler equations (density) for $N_\mathcal{X} = 500$ and DG polynomial degree $K_\mathcal{X} = 3$. Example 4.3.

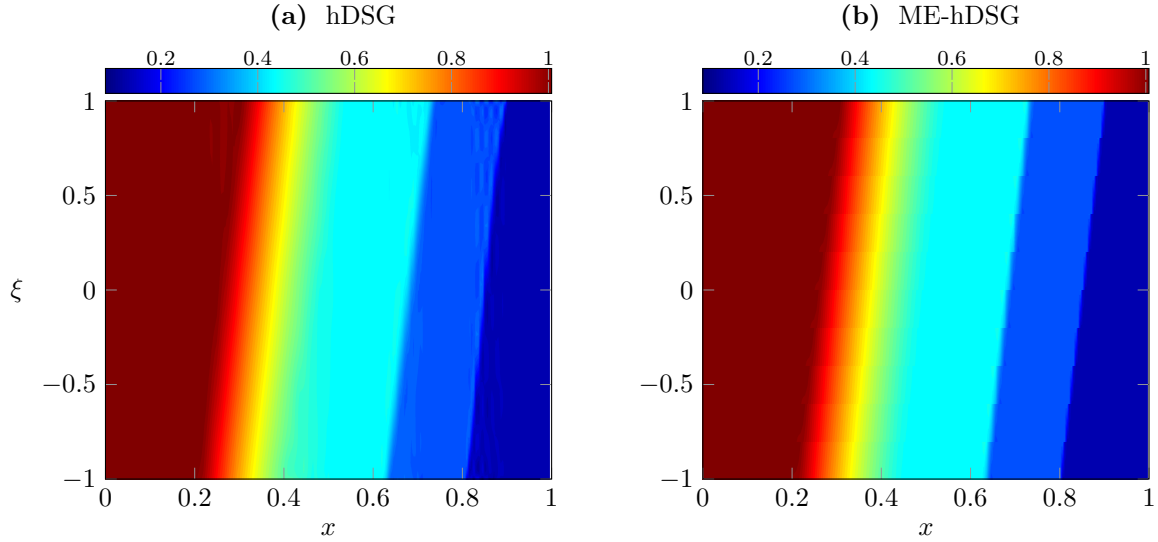


Figure 4: Expected value of the density ρ at $t = 0.2$ for Euler equations with initial state (4.4), $N_\mathcal{X} = 500$, DG polynomial degree $K_\mathcal{X} = 3$. For hDSG, $K_\Gamma = 10$ and for ME-hDSG $K_\Gamma = 1$, $N_\Gamma = 10$. Example 4.3.

K_Γ/N_Γ		1	2	3	4	5	6	7	8	9
hDSG [%]		0.0146	0.1473	0.0721	0.0457	0.0376	0.0386	0.0335	0.0251	0.0199
ME-hDSG [%]		0.0146	0.0028	0.0021	0.0034	0.0037	0.0022	0.0024	0.0021	0.0008

Table 10: Percentage of limited cells over all time-steps for the Euler equations with $N_\mathcal{X} = 500$ and DG polynomial degree $K_\mathcal{X} = 3$. For ME-hDSG we use $K_\Gamma = 1$. Example 4.3

We choose the angle of the ramp uncertain, i.e., we let $\xi \sim \mathcal{U}(28^\circ, 32^\circ)$ and consider the following Riemann

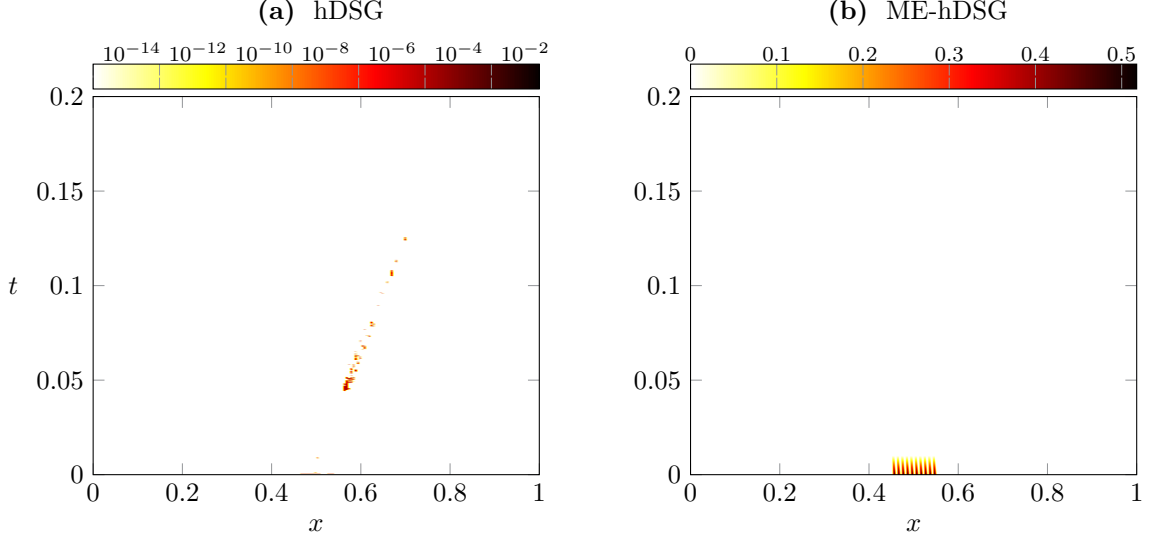


Figure 5: Limiter plot for Euler equations with initial state (4.4), $N_{\mathcal{X}} = 500$ and DG polynomial degree $K_{\mathcal{X}} = 3$. For hDSG, $K_{\Gamma} = 2$ and for ME-hDSG $K_{\Gamma} = 1$, $N_{\Gamma} = 10$. For a better visualization of the hDSG method, we have used a logarithmic z-scale. Example 4.3

data in primitive variables

$$\left. \begin{aligned} \rho(t=0, x, y, \xi) &= \begin{cases} 8, & x < \bar{x} + \tan\left(\frac{\xi\pi}{180^\circ}\right)y, \\ 0.125, & x \geq \bar{x} + \tan\left(\frac{\xi\pi}{180^\circ}\right)y, \end{cases} \\ v_1(t=0, x, y, \xi) &= \begin{cases} 8.25 \cos\left(\frac{\xi\pi}{180^\circ}\right), & x < \bar{x} + \tan\left(\frac{\xi\pi}{180^\circ}\right)y, \\ 0, & x \geq \bar{x} + \tan\left(\frac{\xi\pi}{180^\circ}\right)y, \end{cases} \\ v_2(t=0, x, y, \xi) &= \begin{cases} -8.25 \cos\left(\frac{\xi\pi}{180^\circ}\right), & x < \bar{x} + \tan\left(\frac{\xi\pi}{180^\circ}\right)y, \\ 0, & x \geq \bar{x} + \tan\left(\frac{\xi\pi}{180^\circ}\right)y, \end{cases} \\ p(t=0, x, y, \xi) &= \begin{cases} 116.5, & x < \bar{x} + \tan\left(\frac{\xi\pi}{180^\circ}\right)y, \\ 1, & x \geq \bar{x} + \tan\left(\frac{\xi\pi}{180^\circ}\right)y, \end{cases} \end{aligned} \right\} \quad (4.5)$$

where $\bar{x} = \frac{1}{6}$ is the start of the ramp. The computational domain is $\mathcal{X} = [0, 4] \times [0, 1]$ and we set $T = 0.2$. At the bottom of the domain we employ reflective boundary conditions whereas we prescribe outflow boundary conditions at the right. At the remaining boundaries we apply Dirichlet boundary conditions, which correspond to the physical values. We use the HLLE numerical flux and according to Remark 3.3 we choose the FV sub-cell limiter as spatial limiter $\Lambda\Pi_{\Delta x, \Delta y}$. To detect troubled cells we implement the modified JST indicator as described in [31].

For this numerical example we apply the ME-hDSG method with $N_{\Gamma} = 8$ MEs, SG polynomial degree $K_{\Gamma} = 4$ and $Q_{\Gamma} = 20$. The physical mesh consists of $N_{\mathcal{X}} = 190 \times 40$ cells and we use a DG polynomial degree of $K_{\mathcal{X}} = 4$. In Figure 6 we plot mean and standard deviation of the density at time $T = 0.2$. We can see that the shock front is smeared out because of the variable angle. Thanks to the high-order resolution in physical and stochastic space, small-scale flow features in mean and variance of density are clearly visible. A high standard deviation can be identified around the position of the shock wave. Around $\bar{x} = \frac{1}{6}$, which corresponds to the start position of the ramp, we also observe a high standard deviation.

Figure 7 shows the values of the limiter variable θ in ME one and eight at time $T = 0.2$. We see that the limiter is only active around the shock front. Furthermore, the limited cells vary with the uncertain angle. The plain ME-SG approach without hyperbolicity-preserving limiter crashes immediately after initialization of the initial condition. This shows that our proposed scheme is a reliable and robust method to compute complex flow problems with a high resolution in space, time and stochasticity.

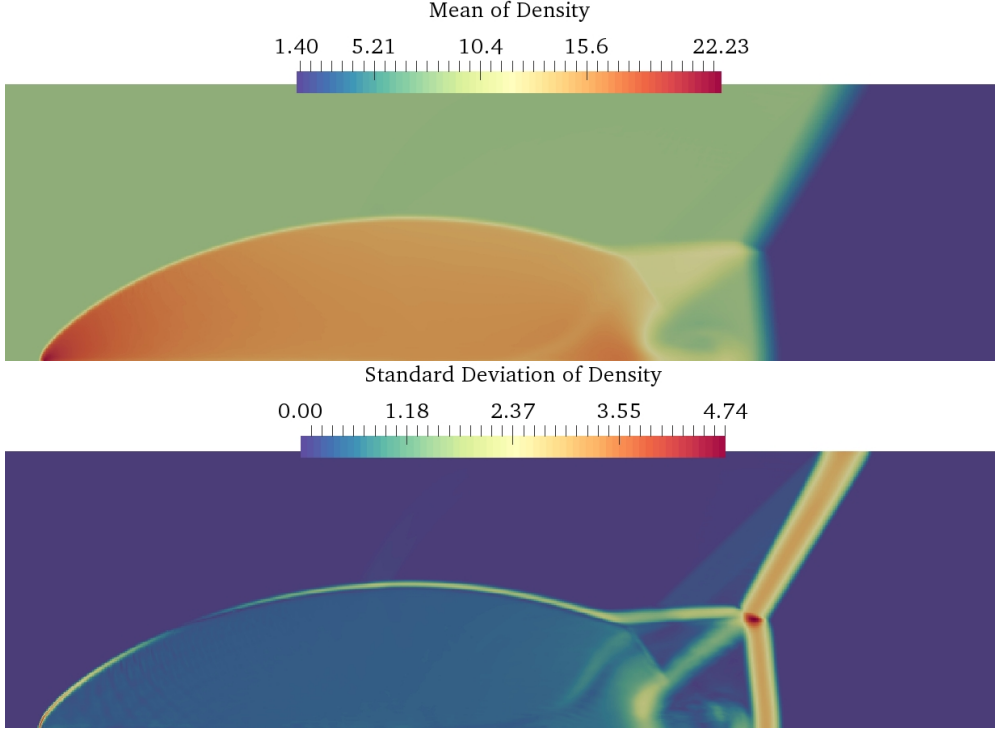


Figure 6: Euler equations with initial state (4.5), $N_{\mathcal{X}} = 7600$ and DG polynomial degree $K_{\mathcal{X}} = 4$. For ME-hDSG, $K_{\Gamma} = 1$, $N_{\Gamma} = 8$. Example 4.4

5. Conclusions and Outlook

Throughout this paper, we have extended the hyperbolicity-preserving stochastic slope limiter from [26] to multiple dimensions in the physical and stochastic space. To derive a high-order method, we combined the hyperbolicity-preserving stochastic Galerkin scheme with a Multi-Element ansatz in the stochastic space and a Runge–Kutta discontinuous Galerkin spatial discretization. The resulting ME-hDSG scheme significantly improved the results compared to the standard stochastic Galerkin scheme, especially when discontinuities are present in the uncertainty. Moreover, we compared the performance of our presented numerical scheme in multiple stochastic dimensions to that of the non-intrusive Stochastic Collocation method. Our results show that our method is competitive in less than three stochastic dimensions, since the cost of the stochastic Galerkin system in higher dimensions is increasing significantly. As final numerical example, we applied our numerical scheme to the Double Mach reflection problem, which in particular shows that our method is capable to handle challenging flow problems.

Future work should incorporate adaptive refinements in space and stochasticity to further improve the efficiency of the ME-hDSG method and to extend the range of dimensions in which the ME-hDSG scheme outperforms non-intrusive methods. Moreover, we want to adopt our methodology to the intrusive polynomial moment method, which promises to require less hyperbolicity limiting.

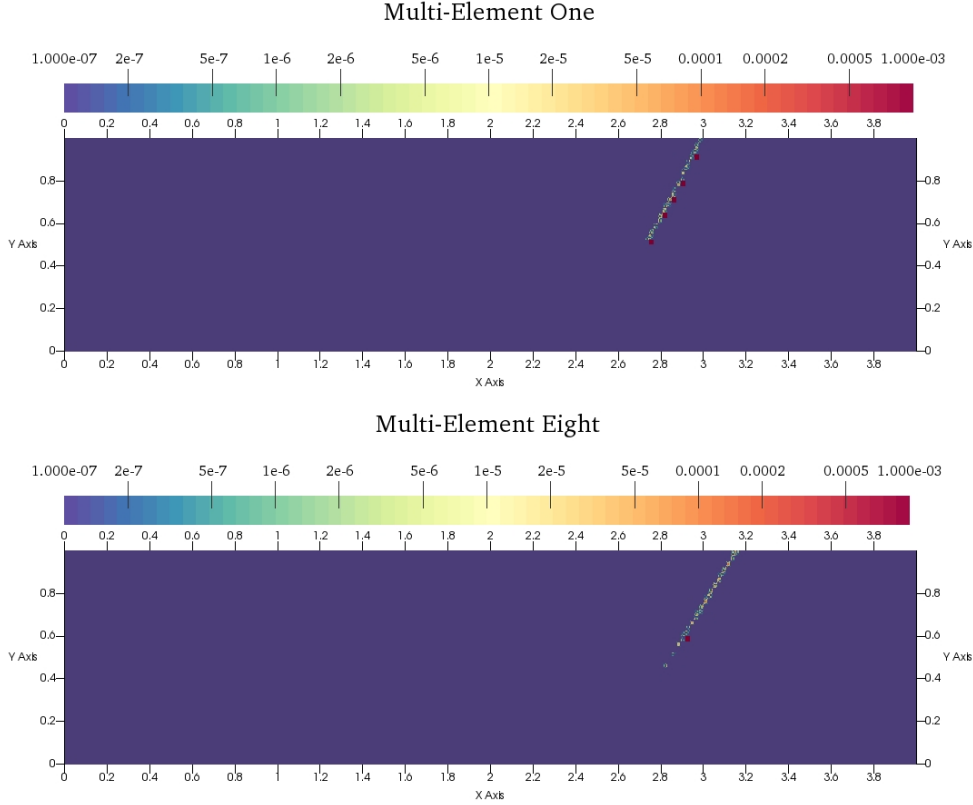


Figure 7: Limiter plot for Euler equations with initial state (4.5), $N_{\mathcal{X}} = 7600$ and DG polynomial degree $K_{\mathcal{X}} = 4$. We plot the usage of the limiter in ME one and eight at time $T = 0.2$. Example 4.4

Acknowledgments

Funding by the Deutsche Forschungsgemeinschaft (DFG) within the RTG GrK 1932 “Stochastic Models for Innovations in the Engineering Science” is gratefully acknowledged. J.D., T.K. and F.M thank the Baden-Württemberg Stiftung for support via the project “SEAL”.

References

- [1] R. ABGRALL AND S. MISHRA, *Uncertainty quantification for hyperbolic systems of conservation laws*, in Handbook of Numerical Analysis, vol. 18, Elsevier, 2017, pp. 507–544.
- [2] B. K. ALPERT, *A class of bases in L^2 for the sparse representation of integral operators*, SIAM J. Math. Anal., 24 (1993), pp. 246–262.
- [3] I. BABUŠKA, R. TEMPONE, AND G. E. ZOURARIS, *Galerkin finite element approximations of stochastic elliptic partial differential equations*, SIAM J. Numer. Anal., 42 (2004), pp. 800–825.
- [4] I. BACKUS, *Sod-shocktube*. <https://github.com/ibackus/sod-shocktube>, 2017.
- [5] T. A. BRUNNER AND J. P. HOLLOWAY, *One-dimensional Riemann solvers and the maximum entropy closure*, Journal of Quantitative Spectroscopy and Radiative Transfer, 69 (2001), pp. 543–566.
- [6] R. BÜRGER, I. KRÖKER, AND C. ROHDE, *A hybrid stochastic Galerkin method for uncertainty quantification applied to a conservation law modelling a clarifier-thickener unit*, ZAMM Z. Angew. Math. Mech., 94 (2014), pp. 793–817.
- [7] R. H. CAMERON AND W. T. MARTIN, *The Orthogonal Development of Non-Linear Functionals in Series of Fourier-Hermite Functionals*, Annals of Mathematics, 48 (1947), pp. 385–392.
- [8] B. COCKBURN AND C.-W. SHU, *Runge-Kutta discontinuous Galerkin methods for convection-dominated problems*, J. Sci. Comput., 16 (2001), pp. 173–261.

- [9] B. DESPRÉS, G. POËTTE, AND D. LUCOR, *Robust uncertainty propagation in systems of conservation laws with the entropy closure method*, in Uncertainty quantification in computational fluid dynamics, vol. 92 of Lect. Notes Comput. Sci. Eng., Springer, Heidelberg, 2013, pp. 105–149.
- [10] B. EINFELDT, C.-D. MUNZ, P. L. ROE, AND B. SJÖGREEN, *On Godunov-type methods near low densities*, J. Comput. Phys., 92 (1991), pp. 273–295.
- [11] R. G. GHANEM AND P. D. SPANOS, *Stochastic finite elements: a spectral approach*, Springer-Verlag, New York, 1991.
- [12] S. GOTTLIEB, *On High Order Strong Stability Preserving Runge–Kutta and Multi Step Time Discretizations*, Journal of Scientific Computing, 25 (2005), pp. 105–128.
- [13] S. GOTTLIEB AND L. GOTTLIEB, *Strong stability preserving properties of Runge–Kutta time discretization methods for linear constant coefficient operators*, Journal of Scientific Computing, 18 (2003).
- [14] F. HINDENLANG, G. J. GASSNER, C. ALTMANN, A. BECK, M. STAUDENMAIER, AND C.-D. MUNZ, *Explicit discontinuous Galerkin methods for unsteady problems*, Comput. & Fluids, 61 (2012), pp. 86–93.
- [15] O. KOLB, *A Third Order Hierarchical Basis WENO Interpolation for Sparse Grids with Application to Conservation Laws with Uncertain Data*, Journal of Scientific Computing, 74 (2018), pp. 1480–1503.
- [16] O. P. LE MAÎTRE AND O. M. KNIO, *Spectral methods for uncertainty quantification: With applications to computational fluid dynamics*, Scientific Computation, Springer, New York, 2010.
- [17] C. D. LEVERMORE, *Relating Eddington factors to flux limiters*, Journal of Quantitative Spectroscopy and Radiative Transfer, 31 (1984), pp. 149–160.
- [18] ———, *Moment closure hierarchies for kinetic theories*, Journal of Statistical Physics, 83 (1996), pp. 1021–1065.
- [19] K. O. LYE, *Multilevel Monte-Carlo for measure valued solutions*, arXiv preprint arXiv:1611.07732, (2016).
- [20] S. MISHRA, N. H. RISEBRO, C. SCHWAB, AND S. TOKAREVA, *Numerical solution of scalar conservation laws with random flux functions*, SIAM/ASA Journal on Uncertainty Quantification, 4 (2016), pp. 552–591.
- [21] S. MISHRA AND C. SCHWAB, *Sparse tensor multi-level Monte Carlo finite volume methods for hyperbolic conservation laws with random initial data*, Mathematics of Computation, 81 (2012), pp. 1979–2018.
- [22] S. MISHRA, C. SCHWAB, AND J. ŠUKYS, *Multi-level Monte Carlo finite volume methods for nonlinear systems of conservation laws in multi-dimensions*, Journal of Computational Physics, 231 (2012), pp. 3365–3388.
- [23] M. P. PETTERSSON, G. IACCARINO, AND J. NORDSTRÖM, *Polynomial chaos methods for hyperbolic partial differential equations: Numerical techniques for fluid dynamics problems in the presence of uncertainties*, Mathematical Engineering, Springer, Cham, 2015.
- [24] P. PETTERSSON, G. IACCARINO, AND J. NORDSTRÖM, *A stochastic Galerkin method for the Euler equations with Roe variable transformation*, J. Comput. Phys., 257 (2014), pp. 481–500.
- [25] G. POËTTE, B. DESPRÉS, AND D. LUCOR, *Uncertainty quantification for systems of conservation laws*, Journal of Computational Physics, 228 (2009), pp. 2443–2467.
- [26] L. SCHLACHTER, *Uncertainty Quantification for Hyperbolic Equations*, TU Kaiserslautern, (2017).
- [27] L. SCHLACHTER AND F. SCHNEIDER, *A hyperbolicity-preserving stochastic Galerkin approximation for uncertain hyperbolic systems of equations*, Journal of Computational Physics, 375 (2018), pp. 80–98.
- [28] F. SCHNEIDER, *Moment models in radiation transport equations*, Dr. Hut Verlag, mathematik ed., 2016.
- [29] F. SCHNEIDER, G. ALLDREDGE, J. KALL, *A realizability-preserving high-order kinetic scheme using WENO reconstruction for entropy-based moment closures of linear kinetic equations in slab geometry*, Kinetic and Related Models, (2015).
- [30] R. C. SMITH, *Uncertainty Quantification: Theory, Implementation, and Applications*, SIAM, 2014.
- [31] M. SONNTAG AND C.-D. MUNZ, *Efficient parallelization of a shock capturing for discontinuous Galerkin methods using finite volume sub-cells*, J. Sci. Comput., 70 (2017), pp. 1262–1289.
- [32] J. TRYÖEN, O. LE MAÎTRE, M. NDJINGA, AND A. ERN, *Intrusive Galerkin methods with upwinding for uncertain nonlinear hyperbolic systems*, J. Comput. Phys., 229 (2010), pp. 6485–6511.
- [33] J. TRYÖEN, O. P. LE MAÎTRE, AND A. ERN, *Adaptive anisotropic spectral stochastic methods for uncertain scalar conservation laws*, SIAM J. Sci. Comput., 34 (2012), pp. A2459–A2481.
- [34] X. WAN AND G. E. KARNIADAKIS, *An adaptive multi-element generalized polynomial chaos method for stochastic differential equations*, J. Comput. Phys., 209 (2005), pp. 617–642.
- [35] ———, *Multi-element generalized polynomial chaos for arbitrary probability measures*, SIAM J. Sci. Comput., 28 (2006), pp. 901–928.
- [36] ———, *Error control in multi-element generalized polynomial chaos method for elliptic problems with random coefficients*, Commun. Comput. Phys., 5 (2009), pp. 793–820.
- [37] N. WIENER, *The homogeneous chaos.*, Amer. J. Math, 60 (1938), pp. 897–936.
- [38] P. WOODWARD AND P. COLELLA, *The numerical simulation of two-dimensional fluid flow with strong shocks*, J. Comput. Phys., 54 (1984), pp. 115–173.
- [39] K. WU, H. TANG, AND D. XIU, *A stochastic Galerkin method for first-order quasilinear hyperbolic systems with uncertainty*, Journal of Computational Physics, 345 (2017), pp. 224–244.
- [40] D. XIU AND J. S. HESTHAVEN, *High-order collocation methods for differential equations with random inputs*, SIAM J. Sci. Comput., 27 (2005), pp. 1118–1139.
- [41] D. XIU AND G. E. KARNIADAKIS, *The Wiener-Askey polynomial chaos for stochastic differential equations*, SIAM J. Sci. Comput., 24 (2002), pp. 619–644.
- [42] Y. YAN, *Galerkin finite element methods for stochastic parabolic partial differential equations*, SIAM J. Numer. Anal., 43 (2005), pp. 1363–1384.
- [43] X. ZHANG AND C.-W. SHU, *On positivity-preserving high order discontinuous Galerkin schemes for compressible Euler equations on rectangular meshes*, J. Comput. Phys., 229 (2010), pp. 8918–8934.